A Robust Optimization Framework for Wildfire Fuel Management

Tomás Lagos[1,*], Nam Ho-Nguyen[1], Dmytro Matsypura[1], and Oleg Prokopyev[2]
[1]Discipline of Business Analytics, The University of Sydney, Sydney, 2000, NSW, Australia,
{tomasignacio.lagos,nam.ho-nguyen,dmytro.matsypura}@sydney.edu.au
[2]Department of Business Administration, University of Zurich, Zurich, 8032, Switzerland, oleg.prokopyev@business.uzh.ch

Abstract: Land agencies plan multi-year prescribed-burn schedules to mitigate catastrophic wildfires, but fuel growth and treatment effectiveness are uncertain and budgets are tight. We study how to allocate treatments over space and time to dismantle high-risk fuel load and landscape connectivity while guaranteeing performance under uncertainty. We develop a robust multi-period optimization model that captures fuel dynamics and decision-dependent treatment effects. The model is easy to calibrate, requiring only two fuel growth parameters, a treatment effect parameter, and the time since the last fire in every location. A new formulation exploits problem structure to reduce model size from cubic to linear dependence in the planning horizon length, enabling large-scale instances. Using the Hawkesbury (NSW, Australia) landscape and fire-history data, robust schedules reduce worst-case high-fuel load and connectivity relative to deterministic plans; the value of robustness grows with planning horizon and uncertainty exposure. Solutions compute quickly, supporting interactive policy exploration. In settings with uncertain parameters, modest robustness strengthens guarantees without materially degrading risk performance. Improvements in estimating treatment effectiveness have the largest impact on losses. Our sensitivity analysis also pinpoints uncertainty ranges within which robust plans perform comparably to deterministic ones, offering clear targets for how much learning is needed to avoid unnecessary conservatism.

Key words: Natural resources, Prescribed burning, Fuel management, Robust optimization, Network-based model

1 Introduction

Wildfires are uncontrolled fires that spread rapidly through vegetation, such as forests, grasslands, or brush. These fires can start from natural causes like lightning or human activities such as campfires, discarded cigarettes, or arson. Wildfires are ubiquitous in areas prone to dry, hot climates, but they are not limited to a particular continent or environment. With climate change leading to higher temperatures and drier conditions, the frequency, severity, and duration of wildfires have been steadily increasing around the globe (World Health Organization 2024).

Although not all wildfires are natural occurrences, the U.S. Environmental Protection Agency (2024) classifies them as natural disasters. Indeed, wildfires can take down more than just forests,

especially when they spread as far as the Californian and Australian wildfires of 2020 or the Canadian wildfires of 2023. During Australia's 2019-2020 fire season, over 46 million acres were burned, causing the loss of approximately one billion animals and numerous endangered species (Ehsani et al. 2020). In 2020, the California August Complex fire burned over 1 million acres and damaged 935 structures (NIFC 2022). In 2023, Canada experienced a record-breaking fire season with over 6.6 thousand wildfires, burning approximately 45.5 million acres across the country (NASA Earth Observatory 2023).

The vast majority of wildfires are triggered by lightning (Igini 2023). While this natural phenomenon is completely unpredictable, adequate land management and fuel treatment planning can significantly diminish the intensity of wildfires. *Prescribed burning*, also known as hazard reduction or controlled burning, plays an essential role in managing wildfires. This practice entails deliberately setting small, low-intensity fires under controlled conditions to eliminate undergrowth, dry grass, and excess vegetation that could otherwise feed larger wildfires. The use of prescribed burning predates modern civilization in many areas worldwide. Indeed, indigenous people of North America and Australia used this land management practice for millennia (Kane 2025).

The early adoption of prescribed burning in Australia was influenced primarily by the understanding that following First Nations land management practices was crucial to mitigate more frequent and severe fires (Morgan et al. 2020). By strategically reducing these *fuels*, the intensity of future fires is diminished, making them more manageable and thereby safeguarding communities, infrastructure, and natural ecosystems. Although the effectiveness of prescribed burning is currently a subject of intense debate, numerous studies argue that the benefits are likely to outweigh the costs (Price and Bradstock 2012, Hunter and Taylor 2022).

1.1 Literature review

As with most natural disasters, wildfires cannot be prevented entirely, and only their effects can be mitigated (Gupta et al. 2016). Previous work on disaster management related to wildfires emphasizes the importance of preventive actions prior to the fire season, including the placement of fire breaks and fuel treatments (Charnley et al. 2015, Martell 2015).

Most studies on fuel treatment optimization use mixed-integer programming (MIP) models (Gillen et al. 2017, and the references therein), starting with the seminal work of Wei et al. (2008). The objective of the model in Wei et al. (2008) is to minimize expected fire loss across the landscape. The landscape is divided into cells, with a probability of fire ignition assigned to each cell. Wei (2012) extends the model of Wei et al. (2008) by replacing the analytic loss function with simulation of

ignitions and burn progression, while Wei and Long (2014) presents a further revision of this model, explicitly aiming to fragment high fire hazard fuel patches.

Numerous other studies follow a similar line of reasoning (e.g., Acuna et al. 2010, Yemshanov et al. 2021). However, they all require a substantial amount of parameter estimation and calibration, which can be a daunting task for practitioners, especially in new environments. As an alternative, Minas et al. (2013) develops a single-period optimization model that jointly determines fuel treatment and suppression resource allocation to maximize area coverage.

All of the models described above are single-period models, which poses a significant limitation because, in practice, the effects of fuel treatments on fire behavior are only temporary (Finney 2001). Furthermore, the long-term goal of hazard reduction is to achieve sustainable ecosystem management through the development and maintenance of desirable landscape-level fuel configurations. This task necessitates a multi-period framework that explicitly models the longevity of individual treatments. To that end, Minas et al. (2014) proposes the first multi-period landscape-level fuel treatment optimization model, with the objective of minimizing the number of cells with high fuel levels. Further refinements of this model appear in Rachmawati et al. (2015, 2016, 2018), León et al. (2023). Although each work improves upon its predecessor, these models are limited by two factors: *(i)* they all use vegetation age as a proxy for the amount of fuel in the cell, and *(ii)* they all implicitly assume that the amount of fuel resets to the same fixed value after each treatment.

Using vegetation age as a proxy for fuel quantity is problematic because it assumes constant fuel accumulation rates, which do not accurately reflect how fuel actually behaves. Empirical studies show that fuel tends to accumulate rapidly in the first several years after a burn, with accumulation rate steadily decreasing in the following years (McCaw 2013). The assumption that fuel quantity resets to a fixed value after each treatment implies that all treatments have the same effect. This contradicts empirical studies, which report that treatment effects can vary substantially (Price et al. 2022).

A comprehensive model is provided by Matsypura et al. (2018), which integrates fuel accumulation, treatment effects, and landscape connectivity. The goal is to minimize the size of potential fires by reducing the connectivity of the network that represents a given landscape. Each node (i.e., each cell) is considered to be either *active* or *inactive*, where the active state implies a sufficiently high fuel load, modeled using the modified Olson fuel accumulation equation. The network connectivity is reduced through fuel treatments that remove a portion of the fuel load, thus rendering the corresponding nodes inactive and deactivating the incident edges. Although the authors conduct a sensitivity analysis of the treatment effectiveness, they do not explicitly address the uncertainty in model parameters.

One approach to address parameter uncertainty, which has been applied to wildfire fuel management, is stochastic optimization (e.g., Bhuiyan et al. 2019, Lagos et al. 2025, and the references therein). However, this approach is highly data-intensive, as it relies on distributional assumptions or requires large amounts of data for calibration. For example, Troncoso et al. (2016) considers a stochastic spatio-temporal forest harvesting problem on flammable landscapes, but does not attempt to develop a mathematical model, citing its complexity. Instead, the authors develop a heuristic algorithm. Evidently, measuring fuel load, treatment effectiveness, and fire ignition distribution with heterogeneous vegetation types poses significant challenges.

Another approach to handling parameter uncertainty is *robust optimization*. In essence, it requires that solutions remain feasible for *all* parameters within a given *uncertainty set*. Robust optimization treats uncertainty without specifying a distribution, making it suitable for settings with limited data availability. In addition, it is typically more tractable than stochastic approaches. In developing our models, we build upon the ideas of Bertsimas and Sim (2004) and Bertsimas and Thiele (2006). The first paper introduces the *budget uncertainty set*, a polyhedral uncertainty set that allows control over the degree of uncertainty via the budget parameter. The second paper explicitly considers a time-varying budget of uncertainty. In both models, due to the polyhedral structure, a linear constraint with a budget uncertainty set permits a linear reformulation.

In certain settings, decisions can influence the size of the uncertainty set. For example, in the context of wildfire management, the longer we plan to leave a cell untreated, the greater our uncertainty about its future fuel load. This phenomenon is known as *decision-dependent uncertainty*. In our methods, we draw on the ideas from Poss (2013) and Nohadani and Sharma (2018), which propose models where binary decisions impact the size of an uncertainty set.

1.2 Main contributions and structure of this work

We introduce a robust multi-period model for fuel treatment optimization based on the setting in Matsypura et al. (2018). Our approach allows us to reduce the complexity of the base model and develop a robust optimization framework. Our model captures fuel dynamics and treatment effectiveness more accurately than existing models in the literature, yet requires estimation of just four parameters: initial fuel load, steady-state fuel load, annual rate of decomposition, and treatment effectiveness. Our contribution to the existing literature is threefold.

Scalability. Our formulation significantly improves scalability and computational efficiency, making it applicable to larger and more complex landscapes. Specifically, our model reduces the number of variables and constraints from $O(nT^3)$ (Matsypura et al. 2018) to $O(nT)$, where n is the number

of cells in the landscape and T is the length of the planning horizon. This model also admits a robust extension for parameter uncertainty; the model in Matsypura et al. (2018) is too complex for this.

Robustness. Unlike the prior work, we explicitly handle uncertainty in fuel accumulation and treatment effectiveness. All fuel treatment optimization models rely on problem parameters that reflect natural phenomena, such as vegetation growth, which governs the effectiveness of treatments in practice. However, estimating these parameters can be challenging, as collecting reliable data and calibrating the parameters accurately is not straightforward. Our work provides a general robust optimization framework, thereby extending the practical applicability of optimization-based fuel treatment planning models by ensuring that solutions remain effective under uncertainty.

Insights. Our numerical study evaluates the robust model across uncertainty sources and treatment budgets, quantifying the trade-offs as uncertainty changes. We find that modest robustness strengthens worst-case guarantees without materially degrading typical performance when parameters are uncertain. Learning priorities emerge: improving estimates of treatment effectiveness has a larger impact on risk reduction than refining fuel-growth inputs, which the robust formulation can absorb at low cost. We also identify practical uncertainty ranges within which robust plans perform comparably to deterministic plans, providing targets for how much accuracy is needed to avoid over conservatism. Finally, robustness is budget-sensitive: as treatment budgets increase, the risk reduction delivered by robust schedules grows relative to deterministic solutions.

The remainder of the paper is structured as follows. In Section 2, we develop the base multi-period deterministic model and present its noisy counterpart. In Section 3, we present our robust framework. Figure 1 provides a summary of the model development process. In Section 4, we examine several objectives that satisfy our modeling assumptions. The computational study is described in Section 5, where we demonstrate the benefits of the robust solutions using historical data from Hawkesbury, New South Wales, Australia. We provide our conclusions in Section 6. The E-Companion includes the proofs, the complete set of computational results, including the scalability study, and other technical details.

2 Deterministic model

In this section, we develop a simplified formulation for the wildfire fuel management problem presented in Matsypura et al. (2018), drastically reducing the number of variables and constraints. We then present a variant of this model when noise is present in the parameters, which serves as a foundation for the development of our robust formulation in Section 3.

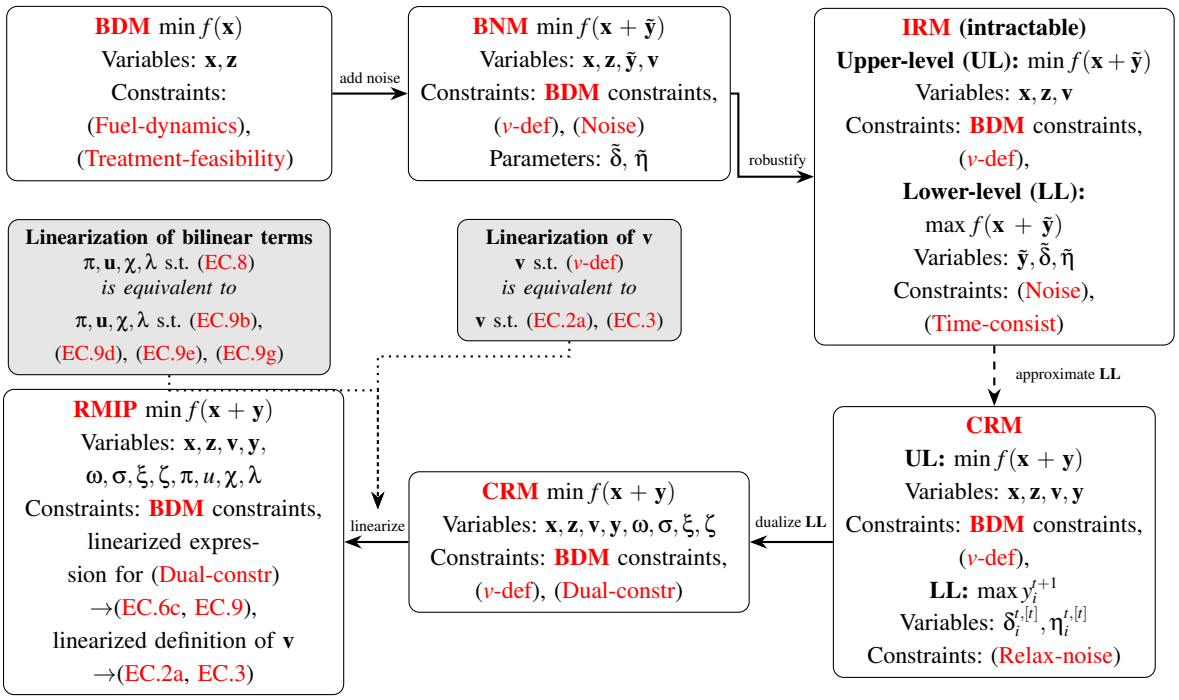

Figure 1 Outline of the model development process in Section 2 and Section 3. The procedures for linearizing the formulation from Section 3 are presented in the gray boxes. These steps are standard techniques in the Integer Programming literature and, therefore, are provided along with the final MIP formulation (**RMIP**) in the E-Companion of this paper. Two examples of objectives f are given in Section 4.

2.1 Fuel dynamics and objective function

Accurate estimation of fuel load is essential for assessing wildfire risk. Prior research suggests that fuel accumulates faster in the initial years after treatment or fire, with the corresponding rates decreasing significantly over the long term. This process can be modeled with the modified Olson fuel accumulation equation (Olson 1963, Watson 2011):

$$x^{\tau} = L^{\text{init}} + (L^{\max} - L^{\text{init}})(1 - e^{-\kappa\tau}) \tag{1}$$

$$= e^{-\kappa}(L^{\text{init}} + (L^{\max} - L^{\text{init}})(1 - e^{-\kappa(\tau-1)})) + (1 - e^{-\kappa})L^{\max}$$

$$= e^{-\kappa}x^{\tau-1} + (1 - e^{-\kappa})L^{\max}, \tag{2}$$

where x^{τ} is the fuel load (in tonnes per hectare, t/ha) τ periods after a fire event, κ is the *decomposition rate of forest litter*, L^{init} (t/ha) is the initial fuel load immediately after the most recent fire, and $L^{\max}$ (t/ha) is the steady-state fuel load, i.e., the equilibrium fuel level attained when the decomposition of litter eventually balances its accumulation (Zazali et al. 2021).

We can simplify equation (2) by defining the *inverse growth rate* $\gamma = e^{-\kappa}$. With this notation, after τ periods of uninterrupted growth, the fuel load is given by the recursion

$$x^{\tau} = \gamma x^{\tau-1} + (1 - \gamma)L^{\max}. \tag{3}$$

This recursion plays a central role in the development of our models.

Consider a simplified scenario with a single area of land. Let x^t be the fuel load at time t, for $t \in [T]$, where T is the planning horizon and $[T] := \{1, 2, \ldots, T\}$. We assume that we are given the initial fuel load x^1, the steady-state fuel load $L^{\max}$, and the inverse growth rate $\gamma \in (0,1)$. Our objective is to determine when to perform fuel treatments in order to mitigate the risk of wildfires. To capture this decision, we introduce binary variables $z^t \in \{0,1\}$ for each $t \in [T]$, with $z^t = 1$ if treatment is performed at time t, and $z^t = 0$ otherwise.

Treatment reduces the fuel load, while not treating allows the fuel to accumulate. Thus, if we decide to treat the area in period t, $z^t = 1$, then the fuel load in the next period is given by $x^{t+1} = \alpha x^t$, where $\alpha \in (0,1)$ is the *treatment effectiveness*, which represents the fraction of fuel load that remains after the treatment (Price et al. 2022). If we decide not to treat the area in period t, then, following equation (3), the fuel load for the next period is $x^{t+1} = \gamma x^t + (1-\gamma)L^{\max}$. Hence, the fuel dynamics can be written as:

$$x^{t+1} = \begin{cases} \alpha x^t, & \text{if} \quad z^t = 1, \\ \gamma x^t + (1-\gamma)L^{\max}, & \text{if} \quad z^t = 0. \end{cases} \tag{4}$$

However, we cannot handle this equation directly, so we reformulate it using Assumption 1.

As outlined in Section 1, the goal of fuel treatment is to eliminate undergrowth, dry grass, and excess vegetation that could otherwise feed larger wildfires. Therefore, a natural objective for our model is to minimize a function $f(\mathbf{x})$ that depends on the amount of fuel in the system $\mathbf{x}$ and measures the size and intensity of potential fires. Since actual fire dynamics involve complex interactions between vegetation, weather, and landscape topology, we work with simplified objectives that allow for a tractable formulation. Specifically, we focus on objectives that satisfy the following assumption:

ASSUMPTION 1. *The objective function $f(\mathbf{x})$ that we minimize (or maximize) is monotone increasing (or decreasing) in $\mathbf{x}$, i.e., if $\mathbf{x} \geq \mathbf{x}'$, then $f(\mathbf{x}) \geq f(\mathbf{x}')$ (or $f(\mathbf{x}) \leq f(\mathbf{x}')$).*

Assumption 1 holds for most natural objectives. One simple example is the total fuel load, i.e., $f(\mathbf{x}) = \|\mathbf{x}\|_1$. We provide more details in Section 4, along with another network-based example. Assumption 1 also allows us to formulate more complex objectives to model specialized problem requirements. For example, if the goal is to protect high-value assets (e.g., farms or critical infrastructure), then we can use a weighted total fuel load, i.e., $f(\mathbf{x}) = \mathbf{w}^\top \mathbf{x}$, with larger weights for the cells containing them to prioritize treatments in those areas.

2.2 Base deterministic model

We now present our base deterministic model. Consider a landscape susceptible to wildfires, divided into a set of cells V, where each cell represents an area available for treatment. Add index $i \in V$ to variables and parameters in equation (4) accordingly. Then, due to Assumption 1 it is sufficient to enforce

$$x_i^{t+1} \geq \begin{cases} \alpha_i x_i^t, & \text{if} \quad z_i^t = 1, \\ \gamma_i x_i^t + (1-\gamma_i) L_i^{\max}, & \text{if} \quad z^t = 0, \end{cases} \tag{5}$$

instead of (4) because the monotonicity ensures that at optimality, the value of x_i^{t+1} is pushed towards the lower bounds. We need the following linear constraints to model inequality (5) :

$$\begin{aligned} x_i^{t+1} &\geq \alpha_i x_i^t, && \forall i \in V,\, t \in [T], \\ x_i^{t+1} &\geq \gamma_i x_i^t + (1-\gamma_i) L_i^{\max} - (1 - \min\{\gamma_i, \alpha_i\})\, L_i^{\max} z_i^t, && \forall i \in V,\, t \in [T], \\ x_i^t &\geq 0, && \forall i \in V,\, t \in [T+1], \\ z_i^t &\in \{0,1\}, && \forall i \in V,\, t \in [T], \end{aligned} \tag{Fuel-dynamics}$$

Another vital relationship that we need to capture is between species' capacity to recover from fire and the interval between successive burns. For example, in dry sclerophyll shrub/grass forests, the minimum acceptable interval between fires is five years, with some species requiring up to 10 years to reach maturity (Kenny et al. 2004). Let $t_i^{\min}$ denote the minimum time required for species to mature, and let t_i^{init} denote the time since the most recent fire at the start of the planning horizon; both parameters are assumed to be known. Then, *(i)* at $t = 1$ the area requires additional $t_i^{\text{start}} = \max\{t_i^{\min} - t_i^{\text{init}}, 0\}$ time periods before it can be considered for treatment. After t_i^{start} periods have passed, we further need to *(ii)* ensure that for each consecutive $t_i^{\min}$ periods there is at most one treatment in the cell. Finally, we need to account for *(iii)* the resource limitations faced by the decision-maker in each period. The parameter b^t represents available resources or budget, while c_i^t denotes the relative difficulty or cost associated with treating cell i. Generally, the decision-maker may have multiple resource constraints in each period, or even constraints over several periods. Consequently, we say that $\mathbf{z} = (z_i^t)_{i \in V, t \in [T]}$ is an operationally feasible treatment schedule if it satisfies constraints *(i), (ii)* and *(iii)* described above:

$$\begin{aligned} z_i^t &= 0, && \forall t \in [t_i^{\text{start}}],\, i \in V, \\ \sum_{s=t}^{\min\{t+t_i^{\min}, T\}} z_i^s &\leq 1, && \forall t \in [\max\{1, T - t_i^{\min}\}] \setminus [t_i^{\text{start}}],\, i \in V, \\ \sum_{i \in V} c_i^t z_i^t &\leq b^t, && \forall t \in [T]. \end{aligned} \tag{Treatment-feasibility}$$

Next, we present the complete formulation for our problem, taking into account multiple geographical areas simultaneously. The *Base Deterministic Model* with a non-decreasing objective function, denoted by $f(\mathbf{x})$, where $\mathbf{x} = (x_i^t)_{i \in V, t \in [T+1]}$, can be expressed as follows:

$$\underset{\mathbf{x},\mathbf{z}}{\text{minimize}} \quad f(\mathbf{x}) \tag{\textbf{BDM}}$$

$$\text{subject to} \quad \text{(Fuel-dynamics)}, \text{(Treatment-feasibility)}.$$

By comparing **BDM** against the model presented in Matsypura et al. (2018), we observe that both models incorporate the same fuel dynamics relationship between $\mathbf{z}$ and $\mathbf{x}$. However, our model offers an advantage by eliminating the need for $nT(T+3)$ variables; the number of variables in our model is only $n(2T+1)$. Constraints (Treatment-feasibility) are common to both models. Our model introduces $2nT$ extra constraints given by (Fuel-dynamics). In contrast, Matsypura et al. (2018) requires an additional $n(T^2+15T+74)T/6$ constraints to model the fuel dynamics. Thus, the total number of constraints in our model is $O(nT)$, whereas in Matsypura et al. (2018), it is $O(nT^3)$.

2.3 Base noisy model

Next, we develop a *noisy* variant of the fuel dynamics given by (4). Specifically, we assume that the estimates of the steady-state fuel load, $L^{\max}$, and the treatment effect, α, are noisy. For now, we also assume that the noise in these parameters is fixed and known. We relax this assumption in Section 3. For exposition, we consider a single cell as we did in Section 2.1.

First, we assume that the noisy steady-state fuel load $\bar{L}^{\max}(t)$ can be different for different periods. The planner observes its noisy estimate $L^{\max}$, and the relationship between the two is

$$\bar{L}^{\max}(t) = (1+\tilde{\eta}^t)L^{\max}$$

where $\tilde{\eta}^t \in [0,1]$ is the *fuel growth noise*.

Here and throughout the paper, we use tilde to denote noisy counterparts of variables (e.g., $\tilde{x}$ for x). Suppose the initial fuel load $\tilde{x}^0 = L^{\text{init}}$ and no treatment is performed. Analogous to (4), the fuel dynamics in the absence of treatment are governed by the following recursion:

$$\tilde{x}^{t+1} = \gamma\tilde{x}^t + (1-\gamma)\bar{L}^{\max}(t).$$

Using this recursion and the definition of x^{t+1} in (4), we have (see details in Section EC.3):

$$\tilde{x}^{t+1} = x^{t+1} + \gamma(\tilde{x}^t - x^t) + (1-\gamma)L^{\max}\tilde{\eta}^t. \tag{6}$$

Next, we allow the treatment to be less effective. In Section 2.2, we model the fuel treatment by reducing the resulting fuel load by a factor of $\alpha \in (0,1)$. In this section, we assume that α is a noisy estimate of the true fuel treatment effectiveness parameter $\bar{\alpha}^t$. It is convenient to parametrize the relationship between the two as

$$1-\bar{\alpha}^t = 1-\alpha-(1-\alpha)\tilde{\delta}^t,$$

where $\tilde{\delta}^t \in [0,1]$ is the *treatment effect noise*. Again, for now, we assume that $\tilde{\delta}^t$ is fixed.

We want to derive the relationship between the noisy fuel load $\tilde{x}^t$, and its post-treatment counterpart $\tilde{x}^{t+1}$. Intuitively, a treatment at time t should result in $\tilde{x}^{t+1} = \bar{\alpha}^t\tilde{x}^t = \tilde{x}^t - (1-\bar{\alpha}^t)\tilde{x}^t$, i.e., a

reduction of the noisy fuel load by a fraction. However, in our setting, this recursion is intractable. So, instead we use its tractable upper bound $\tilde{x}^{t+1} = \tilde{x}^t - (1-\bar{\alpha}^t)x^t$. Thus, we have

$$\tilde{x}^{t+1} = \tilde{x}^t - (1-\bar{\alpha}^t)x^t = \tilde{x}^t - x^t + (\alpha + (1-\alpha)\tilde{\delta}^t)x^t. \tag{7}$$

Putting (6) and (7) together, we can write the noisy fuel dynamics as:

$$\tilde{x}^{t+1} = \begin{cases} \tilde{x}^t - x^t + (\alpha + (1-\alpha)\tilde{\delta}^t)x^t, & \text{if} \quad z^t = 1, \\ x^{t+1} + \gamma(\tilde{x}^t - x^t) + (1-\gamma)L^{\max}\tilde{\eta}^t, & \text{if} \quad z^t = 0, \end{cases}$$

Let $\tilde{y}^t$ denote the *fuel load noise* in the cell at time t, i.e., $\tilde{y}^t = \tilde{x}^t - x^t$. Since $x^{t+1} = \gamma x^t + (1-\gamma)L^{\max}$, the noisy fuel dynamics can be written as follows:

$$\tilde{x}^{t+1} = \begin{cases} \tilde{y}^t + (\alpha + (1-\alpha)\tilde{\delta}^t)x^t, & \text{if} \quad z^t = 1, \\ \gamma(\tilde{y}^t + x^t) + (1-\gamma)L^{\max}(1+\tilde{\eta}^t), & \text{if} \quad z^t = 0. \end{cases} \tag{8}$$

We interpret (8) similar to (4). That is, if we decide to treat, then the total noisy fuel load in the next period is the current fuel load noise $\tilde{y}^t$ plus a noisy proportion $(\alpha + (1-\alpha)\tilde{\delta}^t)$ of the current deterministic load x^t. In contrast, if we decide not to treat, then the total noisy fuel load in the next period is a convex combination with weight γ of the current noisy fuel load $\tilde{y}^t + x^t$ and the noisy steady-state fuel load $L^{\max}(1+\tilde{\eta}^t)$. By equation (4) from (8), we obtain the following equation for the fuel load noise:

$$\tilde{y}^{t+1} = \begin{cases} \tilde{y}^t + (1-\alpha)\tilde{\delta}^t x^t, & \text{if} \quad z^t = 1, \\ \gamma\tilde{y}^t + (1-\gamma)L^{\max}\tilde{\eta}^t, & \text{if} \quad z^t = 0. \end{cases} \tag{9}$$

Observe that $\tilde{y}^{t+1} \geq \tilde{y}^t$ for all $t \in [T]$. Recall that the decision of when to perform fuel treatment in cell $i \in V$ is encoded by vector $\mathbf{z}$, and $\mathbf{x}$ represents the part of the fuel load assumed by the planner at each time $t \in [T+1]$. From (9), we can derive the following relationship between $\mathbf{x}$, $\tilde{\mathbf{y}}$, and $\mathbf{z}$:

$$\tilde{y}_i^{t+1} = \sum_{s=1}^{t} \gamma_i^{\sum_{\tau=s+1}^{t}(1-z_i^\tau)} \left((1-\alpha_i)\tilde{\delta}_i^s x_i^s z_i^s + (1-\gamma_i)L_i^{\max}\tilde{\eta}_i^s(1-z_i^s) \right). \tag{10}$$

Equation (10) is nonlinear due to the terms $x^s z^s$ and $\gamma^{\sum_{\tau=s+1}^{t}(1-z^\tau)}$. To linearize these terms, we introduce additional binary variables

$$v_{i,t}^{s,k} = \begin{cases} 1, & \text{if } \sum_{\tau=s+1}^{t}(1-z_i^\tau) = k, \\ 0, & \text{otherwise.} \end{cases} \tag{v-def}$$

Since $\gamma_i^{\sum_{\tau=s+1}^{t}(1-z_i^\tau)} = \gamma_i^k$ whenever $\sum_{\tau=s+1}^{t}(1-z_i^\tau) = k$, which by ($v$-def) is equivalent to $v_{i,t}^{s,k} = 1$. Consequently, the following equation holds:

$$\gamma_i^{\sum_{\tau=s+1}^{t}(1-z_i^\tau)} = \sum_{k=0}^{t-s} \gamma_i^k v_{i,t}^{s,k}, \qquad \forall i \in V,\, t \in [T],\, s \in [t],$$

and thus, (10) reduces to

$$\tilde{y}_i^{t+1} = \sum_{s=1}^{t} \left(((1-\alpha_i)\tilde{\delta}_i^s x_i^s z_i^s + (1-\gamma_i)L_i^{\max}\tilde{\eta}_i^s(1-z_i^s)) \sum_{k=0}^{t-s} \gamma_i^k v_{i,t}^{s,k} \right), \ \forall i \in V, t \in [T]. \tag{Noise}$$

While (Noise) is still nonlinear, standard techniques can be applied to linearize it; we explain this modeling procedure as well as how to model (v-def) in detail in Section EC.4.

In summary, the noisy counterpart of **BDM**, the *Base Noisy Model*, is given by:

$$\begin{aligned} \underset{\mathbf{x},\tilde{\mathbf{y}},\mathbf{z},\mathbf{v}}{\text{minimize}} \quad & f(\mathbf{x}+\tilde{\mathbf{y}}) && \textbf{(BNM)} \\ \text{subject to} \quad & \text{(Fuel-dynamics)}, \text{(Treatment-feasibility)}, (v\text{-def}), \text{(Noise)}, \end{aligned}$$

where the key difference from **BDM** is the presence of noise modeled via variables $\tilde{\mathbf{y}}$ and $\mathbf{v}$ with additional constraints (v-def) and (Noise).

3 Robust model

This section presents a robust counterpart to the **BNM** model developed in Section 2.3. It provides a principled approach to safeguard our policies against perturbations to the noise terms $\tilde{\delta},\tilde{\eta}$ in the **BNM** model. We think of the parameters $\tilde{\delta},\tilde{\eta}$ as being chosen by "nature" in a way that we cannot anticipate. The robust approach assumes that nature chooses $\tilde{\delta},\tilde{\eta}$ in an *adversarial* manner, i.e., to maximize a minimization-based objective $f(\mathbf{x}+\tilde{\mathbf{y}})$ or vice versa.

While one may argue that a stochastic choice of $\tilde{\delta},\tilde{\eta}$ may be more accurate, we opt for a robust approach because it avoids assumptions about probability distributions of $\tilde{\delta},\tilde{\eta}$. Also, it does not require access to large quantities of empirical data to estimate probability distributions. Even if we had enough data, one could argue that changes in climate can render these estimates uninformative. We begin in Section 3.1 by constructing an *uncertainty set* of perturbations for the $\tilde{\delta},\tilde{\eta}$ parameters from the **BNM** model. In Section 3.2, we develop several robust models, culminating with the linear MIP, which can be solved with an off-the-shelf solver.

3.1 Uncertainty set

We assume that the values of z_i^t and x_i^t are known to nature, which is reasonable since the $\mathbf{z}$-variables represent the fuel treatment plan, while the $\mathbf{x}$ variables represent the deterministic fuel load (Fuel-dynamics). Nature's task is to determine the values of $\tilde{\delta}_i^s$ and $\tilde{\eta}_i^s$ to increase the noisy part of the fuel load $\tilde{\mathbf{y}}$. We provide bounds on the choices that nature may make in the form of the following *decision-dependent budget uncertainty sets*:

$$\Delta_i^t(\mathbf{z}_i) := \left\{ (\tilde{\delta}_i^s,\tilde{\eta}_i^s)_{s\in[t]} : \sum_{s=1}^{t}\tilde{\delta}_i^s \le \Gamma_i^{t,\delta}(\mathbf{z}_i),\ \sum_{s=1}^{t}\tilde{\eta}_i^s \le \Gamma_i^{t,\eta}(\mathbf{z}_i),\ \tilde{\delta}_i^s,\tilde{\eta}_i^s\in[0,1],\ s\in[t] \right\}. \tag{11}$$

These are inspired by the budget uncertainty sets of Bertsimas and Sim (2004), and they give rise to linear robust counterparts. The main difference is that in (11) the budgets of uncertainty $\Gamma_i^{t,\delta}(\mathbf{z}_i)$ and $\Gamma_i^{t,\eta}(\mathbf{z}_i)$ depend on our decisions $\mathbf{z}$. We next discuss how we model these.

We allow the budgets to vary depending on our treatment decisions $\mathbf{z}_i = (z_i^t)_{t\in[T]}$ as follows:

$$\Gamma_i^{t,\delta}(\mathbf{z}_i) = \Gamma_i^{t-1,\delta}(\mathbf{z}_i) + \beta_i^{t,\delta}(1-z_i^t), \qquad \forall i\in V,\ t\in[T], \tag{12a}$$

$$\Gamma_i^{t,\eta}(\mathbf{z}_i) = \Gamma_i^{t-1,\eta}(\mathbf{z}_i) + \beta_i^{t,\eta}(1-z_i^t), \qquad \forall i\in V,\ t\in[T], \tag{12b}$$

where $\beta_i^{t,\delta}$ and $\beta_i^{t,\eta}$ are fixed increments that depend on environmental factors, while $\Gamma_i^{0,\delta}$ and $\Gamma_i^{0,\eta}$ are constants that reflect the initial state of cell i.

The rationale behind this modeling choice is to allow uncertainty to increase over time, similar to the accumulation of errors typical for forecasting models; see Hyndman et al. (2008). Since determining the fuel load in the future is a prediction problem, it is natural to assume that errors increase the further we look into the future. Indeed, the longer we leave a cell untreated, the less we typically know about its current state. If, on the other hand, we were to treat a cell in every period, then the uncertainty would not increase. The structure in (12) reflects this intuition. Furthermore, changing the values of $\beta_i^{t,\delta}$ and $\beta_i^{t,\eta}$ in (12) allows us to control the size of the uncertainty set and, consequently, the *level of robustness* of our solutions.

3.2 Robust formulation

In this section, we present our robust model, where nature selects the worst-case parameters within the uncertainty sets presented in Section 3.1. First, we present our ideal robust setting where nature's selection is *time-consistent*, and then, we present a tractable conservative approximation of it.

A robust approach to tackling the problem implies that nature selects a combination of noise parameters that maximizes the fuel load given the treatment decisions. We say that nature's decision is *time-consistent* if it satisfies the following condition:

$$(\tilde{\delta}_i^s, \tilde{\eta}_i^s)_{s\in[t]} \in \Delta_i^t(\mathbf{z}_i), \qquad \forall i \in V,\, t \in [T]. \tag{Time-consist}$$

That is, nature is time-consistent if its noise allocation satisfies the constraints of all uncertainty sets, which leads to the following *Ideal Robust Model*:

$$\begin{aligned} \underset{\mathbf{x},\mathbf{z},\mathbf{v}}{\text{minimize}} \quad & \max_{\tilde{\mathbf{y}},\tilde{\delta},\tilde{\eta}\text{: (Noise),(Time-consist)}} f(\mathbf{x}+\tilde{\mathbf{y}}) \\ \text{subject to} \quad & \text{(Fuel-dynamics)}, \text{(Treatment-feasibility)}, (v\text{-def}). \end{aligned} \tag{IRM}$$

Next, we illustrate our robust modeling assumptions with a simple example of a single cell.

EXAMPLE 1. Consider a single cell, that is, $|V| = 1$, and let $L^{\max} = 16.4$, $\kappa = 0.17$, $\alpha = 0.51$, $t^{\min} = 10$, $L^{\text{init}} = 0$, and $t^{\text{init}} = 2$. The choice of these parameter values is guided by the real-life case, which we discuss in detail in Section 5. Figure 2 shows the fuel load dynamics for 50 periods with and without treatment for different values of $\beta^\delta, \beta^\eta \in \{0.0, 0.01, 0.02, 0.05\}$, and $(\Gamma_i^{0,\delta}, \Gamma_i^{0,\eta}) = (\beta^\delta t^{\text{init}}, \beta^\eta t^{\text{init}})$. The figure on the left shows the difference in the uninterrupted growth of the fuel. Our model takes into account uncertainty by changing the rate of fuel growth and the corresponding upper bound. The figure on the right shows the effect of noise on fuel load with treatment. We can see that for smaller values of β^δ, i.e., 0.01 and 0.02, nature chose to use the noise to offset the effect of the second, third, and fourth treatments in periods 22, 33, and 44, respectively. Nature's strategy is manifested in modest

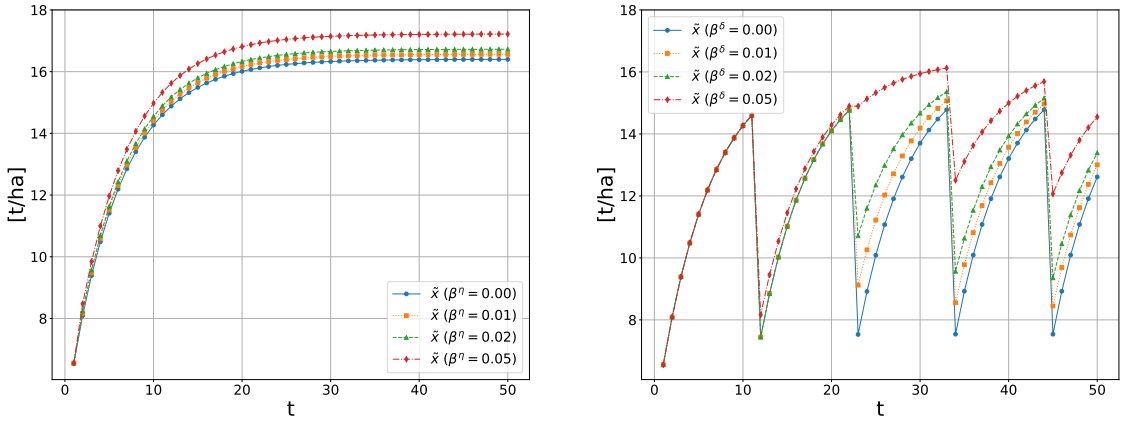

(a) No treatment. (b) Treatment.

Figure 2 Sensitivity of fuel load to different values of $\beta^\delta, \beta^\eta \in \{0.0, 0.01, 0.02, 0.05\}$, with and without treatment in tonnes per hectare; see Example 1. Larger values of β^δ and β^η correspond to larger uncertainty sets for nature's noise allocation. Plot (a) shows the case where no treatment is done with uncertainty in fuel growth; plot (b) shows the case where treatment is performed every 11 periods with uncertainty in treatment effectiveness.

reductions in the corresponding fuel loads and the fact that the corresponding curves overlap with the deterministic case up to period 21. In contrast, for $\beta^\delta = 0.05$, the budget of uncertainty is sufficient to entirely offset fuel reduction due to the second treatment (flat section between periods 21 and 22) and partially offset it before and after the second treatment. These observations suggest that with a higher budget of uncertainty, nature is able to push some components of $\tilde{\delta}$ and $\tilde{\eta}$ to their maximum. □

The **IRM** problem is what we *ideally* would like to solve. Unfortunately, it is not tractable because of the complicated multi-period dependence of f on the components of $\tilde{\mathbf{y}}$. Hence, we relax nature's consistency constraint in a way that allows us to obtain a tractable *conservative* formulation. To do this, we consider new variables δ and η corresponding to $\tilde{\delta}$ and $\tilde{\eta}$, respectively, but having larger dimensionality. As a shorthand, we denote $\tilde{\delta}_i^{[t]} = (\tilde{\delta}_i^s)_{s\in[t]}$, $\tilde{\eta}_i^{[t]} = (\tilde{\eta}_i^s)_{s\in[t]}$, $\delta_i^{t,[t]} = (\delta_i^{t,s})_{s\in[t]}$ and $\eta_i^{t,[t]} = (\eta_i^{t,s})_{s\in[t]}$. We link (δ, η) to $(\tilde{\delta}, \tilde{\eta})$ by identifying $\delta_i^{t,[t]} = \tilde{\delta}_i^{[t]}$ and $\eta_i^{t,[t]} = \tilde{\eta}_i^{[t]}$ for all $i \in V$, $t \in [T]$. Thus, nature's time-consistency is enforced by:

$$(\delta_i^{t,[t]}, \eta_i^{t,[t]}) \in \Delta_i^t(\mathbf{z}_i), \qquad \forall i \in V,\ t \in [T], s \in [t], \tag{13a}$$

$$\delta_i^{t,s} = \delta_i^{t+1,s},\ \eta_i^{t,s} = \eta_i^{t+1,s}, \qquad \forall i \in V,\ t \in [T-1], s \in [t]. \tag{13b}$$

See Section EC.5 in the E-Companion for an example.

To obtain a tractable model, we relax condition (13b) while keeping (13a) and use y_i^t to denote the relaxed (conservative) amount of noise. Our relaxation makes each expression of y_i^{t+1} component-wise independent:

$$y_i^{t+1} = \max_{(\delta_i^{t,[t]},\eta_i^{t,[t]})\in\Delta_i^t(\mathbf{z}_i)} \left\{ \sum_{s=1}^{t} \left(\left((1-\alpha_i)\delta_i^{t,s} x_i^s z_i^s + (1-\gamma_i) L_i^{\max} \eta_i^{t,s} (1-z_i^s) \right) \times \sum_{k=0}^{t-s} \gamma_i^k v_{i,t}^{s,k} \right) \right\}, \quad \forall i \in V,\ t \in [T], \tag{Relax-noise}$$

which leads to a tractable robust model with *row-wise independent uncertainty*. Hence, each element of $\mathbf{y} = (y_i^t)_{i\in V, t\in[T+1]}$ can be maximized independently. Since $f(\mathbf{x}+\mathbf{y})$ is monotone non-decreasing in $\mathbf{y}$, we can solve the following *Conservative Robust Model*:

$$\begin{aligned} \underset{\mathbf{x},\mathbf{y},\mathbf{z},\mathbf{v}}{\text{minimize}} \quad & f(\mathbf{x}+\mathbf{y}) \\ \text{subject to} \quad & \text{(Fuel-dynamics)}, \text{(Treatment-feasibility)}, \\ & (v\text{-def}), \text{(Relax-noise)}. \end{aligned} \tag{CRM}$$

This relaxation is a conservative approximation (see proof of Proposition 1 in Section EC.5).

PROPOSITION 1. *Under Assumption 1, the optimal value of **CRM** provides an upper bound for **IRM**.*

Now, we reformulate **CRM** by dualizing the subproblem containing the variables associated with nature in the uncertainty set $\Delta_i^t(\mathbf{z}_i)$. Observe that nature's maximization problem in (Relax-noise), for each $t \in [T]$ and $i \in V$, can be expressed as follows:

$$\begin{aligned} \underset{\delta_i^{t,[t]},\eta_i^{t,[t]}}{\text{maximize}} \quad & \sum_{s=1}^{t} \left(\left((1-\alpha_i) x_i^s z_i^s \delta_i^{t,s} + (1-\gamma_i) L_i^{\max} (1-z_i^s) \eta_i^{t,s} \right) \sum_{k=0}^{t-s} \gamma_i^k v_{i,t}^{s,k} \right) \\ \text{subject to} \quad & \sum_{s=1}^{t} \delta_i^{t,s} \le \Gamma_i^{t,\delta}(\mathbf{z}_i), \quad \sum_{s=1}^{t} \eta_i^{t,s} \le \Gamma_i^{t,\eta}(\mathbf{z}_i), && (\omega_i^t, \sigma_i^t \ge 0) \\ & \delta_i^{t,s}, \eta_i^{t,s} \in [0,1], \quad \forall s \in [t]. && (\xi_i^{t,s}, \zeta_i^{t,s} \ge 0) \end{aligned}$$

Here, $\xi_i^{t,s}$ and $\zeta_i^{t,s}$ are the dual variables corresponding to the upper bounds of the variables $\delta_i^{t,s}$ and $\eta_i^{t,s}$, respectively, and ω_i^t and σ_i^t are the dual variables associated with the corresponding nature's noise budgets constraint on $\delta_i^{t,s}$ and $\eta_i^{t,s}$, respectively. The reader can verify that the dual for the above problem is as follows:

$$\begin{aligned} \underset{\omega_i^t,\sigma_i^t,\xi_i^{t,[t]},\zeta_i^{t,[t]}}{\text{minimize}} \quad & \Gamma_i^{t,\delta}(\mathbf{z}_i)\omega_i^t + \Gamma_i^{t,\eta}(\mathbf{z}_i)\sigma_i^t + \sum_{s=1}^{t} (\xi_i^{t,s} + \zeta_i^{t,s}) \\ \text{subject to} \quad & \sigma_i^t + \zeta_i^{t,s} \ge (1-\gamma_i) L_i^{\max} (1-z_i^s) \sum_{k=0}^{t-s} \gamma_i^k v_{i,t}^{s,k}, && \forall s \in [t], \\ & \omega_i^t + \xi_i^{t,s} \ge (1-\alpha_i) x_i^s z_i^s \sum_{k=0}^{t-s} \gamma_i^k v_{i,t}^{s,k}, && \forall s \in [t], \\ & \omega_i^t, \sigma_i^t, \xi_i^{t,s}, \zeta_i^{t,s} \ge 0, && \forall s \in [t]. \end{aligned} \tag{Dual-consist}$$

Then, using strong duality, we find the following robust nonlinear reformulation of **CRM**:

$$\begin{aligned} \underset{\mathbf{x},\mathbf{y},\mathbf{z},\mathbf{v}}{\text{minimize}} \quad & f(\mathbf{x}+\mathbf{y}) \\ \text{subject to} \quad & \text{(Fuel-dynamics)}, \text{(Treatment-feasibility)}, (v\text{-def}), \end{aligned} \tag{14a}$$

$$y_i^{t+1} = \min_{\omega_i^t, \sigma_i^t, \xi_i^{t,[t]}, \zeta_i^{t,[t]}} \quad \Gamma_i^{t,\delta}(\mathbf{z}_i)\omega_i^t + \Gamma_i^{t,\eta}(\mathbf{z}_i)\sigma_i^t + \sum_{s=1}^{t}(\xi_i^{t,s} + \zeta_i^{t,s}) \qquad \forall i \in V,\ t \in [T]. \tag{14b}$$
$$\text{subject to} \quad \text{(Dual-consist)},$$

Under Assumption 1, and since the $\mathbf{y}$-constraints are variable-disjoint, we can lift the "min" term in equation (14b) and let the minimization in (14a) control variables ω, σ, ξ and ζ. Specifically, we use the fact that there are no common variables between the constraints that determine the values of the elements of $\mathbf{y}$, and the planner wants to have each element of $\mathbf{y}$ as small as possible. Hence, any optimal solution $(\omega_i^t, \sigma_i^t, \xi_i^{t,[t]}, \zeta_i^{t,[t]})$ to (14b) is optimal for the problem having these variables lifted. Thus, we obtain the following reformulation of (14):

$$\underset{\mathbf{x},\mathbf{y},\mathbf{z},\mathbf{v},\omega,\sigma,\xi,\zeta}{\text{minimize}} \quad f(\mathbf{x}+\mathbf{y}) \tag{Single-level-\textbf{CRM}}$$
$$\text{subject to} \quad \text{(Fuel-dynamics)}, \text{(Treatment-feasibility)}, \text{(}v\text{-def)},$$
$$y_i^{t+1} = \Gamma_i^{t,\delta}(\mathbf{z}_i)\omega_i^t + \Gamma_i^{t,\eta}(\mathbf{z}_i)\sigma_i^t + \sum_{s=1}^{t}(\xi_i^{t,s} + \zeta_i^{t,s}), \qquad \forall i \in V,\ t \in [T]. \tag{Dual-constr}$$
$$\text{(Dual-consist)},$$

Observe that formulation Single-level-**CRM** is non-linear. In Sections EC.6 and EC.7 of the E-Companion, we show how to linearize Single-level-**CRM** and **IRM**. Our derivations allow us to obtain a compact MIP formulation for **CRM**, thereby keeping the tractability of the deterministic model presented in Section 2.2.

4 Objectives

In this section, we present two objective functions f that can be used in our setting. The first one simply minimizes the total fuel load, whereas the second aims to break vegetation connectivity patterns to reduce the spread and the size of potential wildfires.

4.1 General framework

There are two tasks we wish to perform with our model: (*i*) determining an optimal treatment plan, where we choose $(\mathbf{x}, \mathbf{z})$ to minimize our objective f; and (*ii*) evaluating a *fixed* treatment plan $(\mathbf{x}, \mathbf{z})$ by maximizing $f(\mathbf{x}+\tilde{\mathbf{y}})$ over possible perturbations $\tilde{\mathbf{y}}$ of the deterministic fuel load $\mathbf{x}$. Therefore, we employ two representations of the objective function f: first, a *minimization* form to compute a treatment policy (with **BDM** or **CRM**):

$$f(\tilde{\mathbf{x}}) = \min_{\mathbf{p}\in\mathcal{P}} \left\{ \mathbf{a}^\top \mathbf{p} \colon h(\tilde{\mathbf{x}}, \mathbf{p}) \geq 0 \right\}; \tag{15}$$

and second, a *maximization* form to evaluate it (with **IRM**):

$$f(\tilde{\mathbf{x}}) = \max_{\mathbf{q}\in Q} \left\{ \mathbf{b}^\top \mathbf{q} \colon g(\tilde{\mathbf{x}}, \mathbf{q}) \leq 0 \right\}. \tag{16}$$

Here, $\mathcal{P}$, Q are mixed-integer linear sets, $\mathbf{a}, \mathbf{b}$ are objective vectors, and g, h are some affine mappings.

To compute a treatment policy $(\mathbf{x}, \mathbf{z})$ for the min-type representation of f in (15), the variables $\mathbf{p}$ can be lifted to the planner's **BDM** problem as follows:

$$\begin{array}{ll} \underset{\mathbf{x},\mathbf{z}}{\text{minimize}} & f(\mathbf{x}) \\ \text{subject to} & \text{(Fuel-dynamics)}, \\ & \text{(Treatment-feasibility)}. \end{array} \quad \Longleftrightarrow \quad \begin{array}{ll} \underset{\mathbf{x},\mathbf{z},\mathbf{p}}{\text{minimize}} & \mathbf{a}^\top \mathbf{p} \\ \text{subject to} & \text{(Fuel-dynamics)}, \\ & \text{(Treatment-feasibility)}, \\ & \mathbf{p} \in \mathcal{P},\ h(\mathbf{x},\mathbf{p}) \geq 0, \end{array}$$

and to the planner's **CRM** problem as follows:

$$\begin{array}{ll} \underset{\substack{\mathbf{x},\mathbf{y},\mathbf{z},\mathbf{v},\mathbf{u},\\ \omega,\xi,\zeta}}{\text{minimize}} & f(\mathbf{x}+\mathbf{y}) \\ \text{subject to} & \text{(Fuel-dynamics)}, \\ & \text{(Treatment-feasibility)}, \\ & (v\text{-def}), (\text{Dual-constr}). \end{array} \quad \Longleftrightarrow \quad \begin{array}{ll} \underset{\substack{\mathbf{x},\mathbf{y},\mathbf{z},\mathbf{v},\mathbf{u},\\ \omega,\xi,\zeta,\mathbf{p}}}{\text{minimize}} & \mathbf{a}^\top \mathbf{p} \\ \text{subject to} & \text{(Fuel-dynamics)}, \\ & \text{(Treatment-feasibility)}, \\ & (v\text{-def}), (\text{Dual-constr}), \\ & \mathbf{p} \in \mathcal{P},\ h(\mathbf{x}+\mathbf{y},\mathbf{p}) \geq 0. \end{array}$$

In both cases, the resulting formulation on the right is a single-level MIP that can be solved using a general-purpose MIP solver.

To evaluate a given policy $(\mathbf{x},\mathbf{z})$, we use the max-type representation (16) and solve nature's maximization problem in **IRM** by lifting the variables $\mathbf{q}$ as follows:

$$\begin{array}{ll} \underset{\tilde{\mathbf{y}},\tilde{\delta},\tilde{\eta}}{\text{maximize}} & f(\mathbf{x}+\tilde{\mathbf{y}}) \\ \text{subject to} & \text{(Noise)}, (\text{Time-consist}). \end{array} \quad \Longleftrightarrow \quad \begin{array}{ll} \underset{\tilde{\mathbf{y}},\tilde{\delta},\tilde{\eta},\mathbf{p}}{\text{maximize}} & \mathbf{b}^\top \mathbf{q} \\ \text{subject to} & \text{(Noise)}, (\text{Time-consist}), \\ & \mathbf{q} \in \mathcal{Q},\ g(\mathbf{x}+\tilde{\mathbf{y}},\mathbf{q}) \leq 0. \end{array}$$

Again, the resulting formulation on the right is a single-level MIP, which can be solved using a general-purpose MIP solver.

In the following subsections, we provide both min- and max-type representations for two objective functions f. These representations allow us to extend the **BDM** and **CRM** models, as well as evaluate the treatment plans under the ideal robust model **IRM**.

4.2 Fuel load-based objective function

Our first objective is to minimize the total fuel load:

$$f(\tilde{\mathbf{x}}) = \|\tilde{\mathbf{x}}\|_1 = \|\mathbf{x}\|_1 + \|\tilde{\mathbf{y}}\|_1.$$

Minimization (planner's problem). Using the lifting procedure described above, we can solve **CRM** to find a robust treatment policy. However, because this objective is linear in noise parameters $\tilde{\delta}$ and $\tilde{\eta}$, we do not have to use conservative approximation. Instead, we can use strong duality on nature's maximization problem in **IRM** and solve the ideal setting exactly. To do this, first, we use equation (Noise) to rewrite $f(\tilde{\mathbf{x}})$ in a more convenient form:

$$f(\tilde{\mathbf{x}}) = \|\mathbf{x}\|_1 + \sum_{i\in V, s\in[T]} \left(\left((1-\alpha_i)\tilde{\delta}_i^s x_i^s z_i^s + (1-\gamma_i) L_i^{\max} \tilde{\eta}_i^s (1-z_i^s) \right) \sum_{t=s}^{T} \sum_{k=0}^{t-s} \gamma_i^k v_{i,t}^{s,k} \right). \tag{17}$$

Then, we dualize nature's maximization problem in **IRM**. Recall that nature's problem is:

$$\begin{aligned} \underset{\tilde{\mathbf{y}},\tilde{\delta},\tilde{\eta}}{\text{maximize}} \quad & f(\mathbf{x}+\tilde{\mathbf{y}}) \\ \text{subject to} \quad & \text{(Noise)}, \text{(Time-consist)}. \end{aligned}$$

The resulting dual is nearly identical to (Dual-consist), except that the dual constraints are associated with $\tilde{\eta}$ and $\tilde{\delta}$ from **IRM**, rather than η and δ from **CRM**. Additionally, the dual variables $\tilde{\xi}_i^s$ and $\tilde{\zeta}_i^s$ are associated with the upper bounds of the components of $\tilde{\delta}$ and $\tilde{\eta}$. Hence, the dual constraints of the nature's maximization problem in this case are:

$$\begin{aligned} \sum_{t=s}^{T} \sigma_i^t + \tilde{\zeta}_i^s &\geq (1-\gamma_i) L_i^{\max} (1-z_i^s) \sum_{k=0}^{t-s} \gamma_i^k v_{i,t}^{s,k}, && \forall i \in V,\ s \in [T], \\ \sum_{t=s}^{T} \omega_i^t + \tilde{\xi}_i^s &\geq (1-\alpha_i) x_i^s z_i^s \sum_{k=0}^{t-s} \gamma_i^k v_{i,t}^{s,k}, && \forall i \in V,\ s \in [T], \\ \omega_i^s, \sigma_i^t, \tilde{\xi}_i^s, \tilde{\zeta}_i^s &\geq 0 && \forall i \in V,\ s \in [T]. \end{aligned} \tag{Ideal-dual}$$

Consequently, the expression for $f(\tilde{\mathbf{x}})$ in this setting is the following LP:

$$f(\mathbf{x},\mathbf{z},\mathbf{v}) = \|\mathbf{x}\|_1 + \min_{\omega,\sigma,\tilde{\xi},\tilde{\zeta}} \left\{ \sum_{i\in V, t\in[T]} \left(\Gamma_i^{t,\delta}(\mathbf{z}_i)\omega_i^t + \Gamma_i^{t,\eta}(\mathbf{z}_i)\sigma_i^t + \tilde{\xi}_i^t + \tilde{\zeta}_i^t \right) : \text{(Ideal-dual)} \right\}. \tag{18}$$

We present the complete resulting formulation in Section EC.7 of the E-Companion.

Maximization (nature's problem). To assess a given policy $(\mathbf{x},\mathbf{z})$, we solve nature's maximization problem in **IRM** with respect to variables $(\tilde{y},\tilde{\delta},\tilde{\eta})$. Formally, the problem is:

$$f^{\text{IRM}}(\mathbf{x},\mathbf{z},\mathbf{v}) = \|\mathbf{x}\|_1 + \max_{\tilde{y},\tilde{\delta},\tilde{\eta}} \left\{ \|\tilde{y}\|_1 : \text{(Noise)}, \text{(Time-consist)} \right\}. \tag{19}$$

Here nature selects coefficients that maximize the planner's objective, taking $\mathbf{z},\mathbf{x},\mathbf{v}$ as given.

4.3 Number of active edges

Our second objective is to break vegetation connectivity patterns. As pointed out by Minas et al. (2014), it is difficult to predict where a fire may start and how it spreads thereafter. Therefore, minimizing the number of active edges in the network induced by the landscape can be interpreted as aiming to break the available fuel into patches and create a mosaic of different post-fire states. This objective aligns well with the traditional practices of Australia's First Nations and echoes our ultimate goal of preventing wildfires from turning into disasters.

We follow the setup of Matsypura et al. (2018) and introduce a graph $G=(V,E)$ induced by the landscape with a set of nodes V and a set of edges E. Each node $i \in V$ corresponds to a cell of the landscape, while $(i,j) \in E$ is created if i and j are adjacent. For example, the network representation of the data we use in our numerical study is presented in Figure 3.

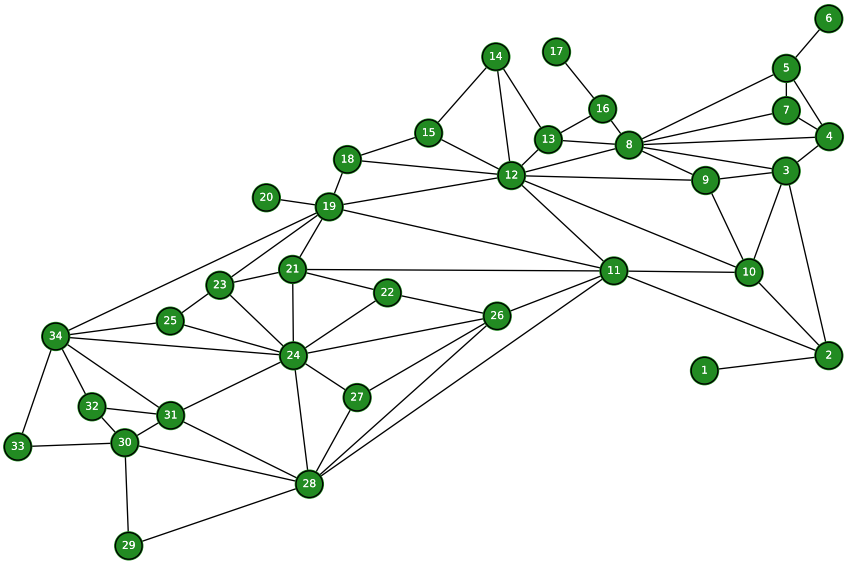

Figure 3 Network representation of the landscape used in Example 2 and Section 5.

A node is *active* if the fuel load of the corresponding cell exceeds a predefined threshold L^{thr}. To model this, we define binary variables θ_i^t, where $\theta_i^t = 1$ if and only if $\tilde{x}_i^t \geq L_i^{\text{thr}}$. The relationship between $\tilde{\mathbf{x}}$ and θ can be enforced via the following set of linear constraints:

$$\tilde{x}_i^t \leq (2L_i^{\max} - L_i^{\text{thr}})\theta_i^t + L_i^{\text{thr}}, \qquad \forall i \in V, \quad t \in [T+1], \tag{20a}$$

$$\tilde{x}_i^t \geq L_i^{\text{thr}}\theta_i^t, \qquad \forall i \in V, \quad t \in [T+1], \tag{20b}$$

$$\theta_i^t \in \{0,1\}, \qquad \forall i \in V, \quad t \in [T+1]. \tag{20c}$$

The choice of $2L_i^{\max}$ in (20a) is justified in Remark EC.1 (E-Companion; Section EC.3).

If two adjacent nodes are active, then the edge between them is *active*. Otherwise, the edge is *inactive*. An active edge indicates that fire can spread between adjacent cells if the fuel load in both cells is sufficient to support it. As treatment is applied to some cells, a portion of the fuel is removed, which can lead to the deactivation of some nodes and all edges incident to them. At the same time, those cells where treatment was not applied continue to accumulate fuel.

We need the following auxiliary variables to model this dynamic: for all $(i,j) \in E$, define $\varepsilon_{i,j}^t \in \{0,1\}$, where $\varepsilon_{i,j}^t = 1$ if and only if $\theta_i^t = \theta_j^t = 1$, i.e., if edge (i,j) is active at time t. The relationship between θ and ε can be enforced through the following set of linear constraints:

$$\varepsilon_{i,j}^t \geq \theta_i^t + \theta_j^t - 1, \qquad \forall t \in [T+1], \quad (i,j) \in E, \tag{21a}$$

$$\varepsilon_{i,j}^t \leq \theta_i^t, \quad \varepsilon_{i,j}^t \leq \theta_j^t, \qquad \forall t \in [T+1], \quad (i,j) \in E, \tag{21b}$$

$$\varepsilon_{i,j}^t \in [0,1], \qquad \forall t \in [T+1], \quad (i,j) \in E. \tag{21c}$$

Note that we can relax binary constraints on $\varepsilon_{i,j}^t$ provided that $\theta_i^t, \theta_j^t \in \{0,1\}$.

Minimization (planner's problem). Using the variables and constraints above, we obtain a robust treatment policy by solving **CRM** with the following objective in minimization form:

$$f(\tilde{\mathbf{x}}) = \min_{\theta,\varepsilon} \{\|\varepsilon\|_1 : (20), (21)\}. \tag{22}$$

Note that if noise is absent and we want to compute a deterministic policy by solving **BDM**, $\tilde{x}_i^t$ should be replaced by x_i^t in (20).

Maximization (nature's problem). To assess the performance of the policies using **IRM**, we write the max-type representation of the objective as:

$$f(\tilde{\mathbf{x}}) = \max_{\theta,\varepsilon} \{\|\varepsilon\|_1 : (20), (21)\}, \tag{23}$$

where $\tilde{x}_i^t$ should be replaced in (20) by $x_i^t + \tilde{y}_i^t$. Nature's objective in (23) is the opposite of the planner's in (22): instead of minimizing the number of active edges, nature seeks to activate as many of them as possible throughout the planning horizon. Then, the max operator in (23) can be lifted to nature's problem, which controls the parameters $\tilde{\delta}$ and $\tilde{\eta}$. Consequently, the performance of treatment policy $(\mathbf{x}, \mathbf{z})$ is given by the optimal value of the following system:

$$f^{\text{IRM}}(\mathbf{x}, \mathbf{z}, \mathbf{v}) = \max_{\tilde{\mathbf{y}},\tilde{\delta},\tilde{\eta},\theta,\varepsilon} \{\|\varepsilon\|_1 : (\text{Noise}), (\text{Time-consist}), (20), (21)\}. \tag{24}$$

Finally, each edge may carry weights reflecting its importance to be active/inactive for the planner's and nature's objectives presented here (recall our discussion in Section 2.1).

EXAMPLE 2. We use real-life data to illustrate the benefits of our robust framework. To improve readability, we use the notation $(\hat{\beta}^\delta, \hat{\beta}^\eta)$ for the parameters used to compute a policy and $(\beta^\delta, \beta^\eta)$ for the parameters used to assess the policy. We show two policies with objective (22), obtained by solving **BDM** (deterministic case, $\hat{\beta}_i^{t,\delta} = \hat{\beta}_i^{t,\eta} = 0$) and **CRM** (robust case, $\hat{\beta}_i^{t,\delta} = \hat{\beta}_i^{t,\eta} = 0.02$). For evaluation we use problem (24) with $\beta^\delta = \beta^\eta = 0.02$.

We use the landscape data, and the associated parameter values of the Hawkesbury region of NSW, Australia, sourced from NSW Rural Fire Services (2016). Specifically, we have $|V| = 34$, $|E| = 71$ (see Figure 3), with the treatment budget $b_t = 5$, and the planning horizon $T = 5$, the threshold for node activation $L_i^{\text{thr}} = 13.4$, the steady state fuel load $L_i^{\max} = 16.4$, and the treatment effect parameter $\alpha_i = 0.51$. Initial maturities, i.e., parameter t^{init} are presented in Table EC.3 in Section EC.8 of the E-Companion. The choice of parameter values is based on local vegetation and is discussed in detail in Section 5.

We present the resulting treatment policies in Figure 4, deterministic on the left and robust on the right. The initial number of active edges is 40 in both cases. For the deterministic policy, this number decreases to 20 in $t = 2$, then increases to 46 in $t = 3$, and it is 32 in $t = 4$. For the robust policy, this number decreases to 23 at $t = 2$, then increases to 38 at $t = 3$, and then it is 21 at $t = 4$. In this case, the improvement offered by the robust solution is about 12%. □

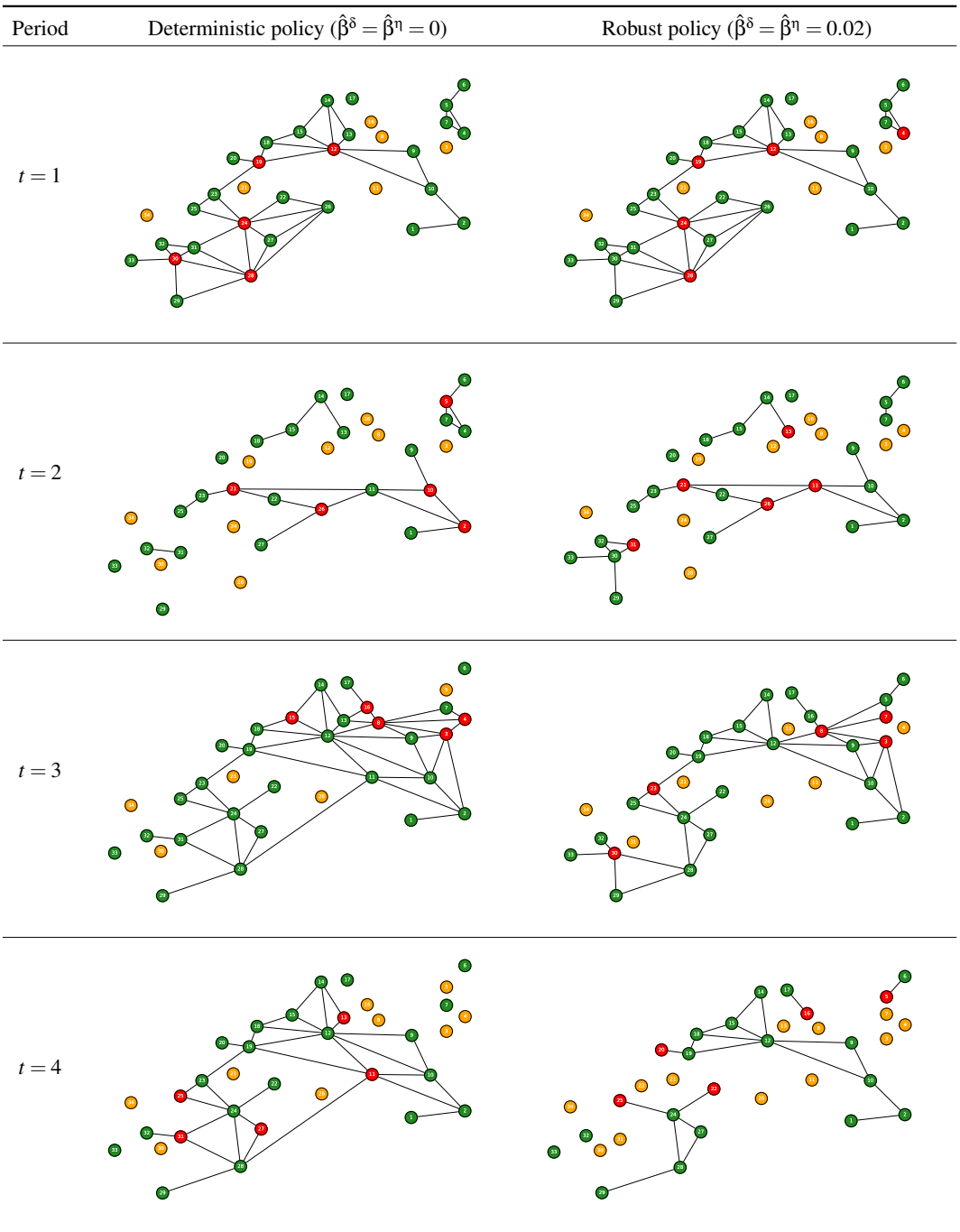

Figure 4 Minimizing active edges: deterministic vs. robust optimal policies under (**IRM**) for the objective (24) with $\beta^{\delta} = \beta^{\eta} = 0.02$. Node colors: red = treated; yellow = fuel below threshold; green = fuel above threshold; $L_i^{\text{thr}} = 13.4$.

5 Numerical study

This numerical study aims to demonstrate the benefits of our robust framework, assess its scalability, and obtain practical insights. We ground the evaluation in a real-world landscape with literature-

validated parameters for that specific area; see Section 5.1. We discuss our findings in Section 5.2. For the complete set of computational results and the scalability study on real and simulated landscapes, see Section EC.9 of the E-Companion.

All experiments were implemented in Python 3.7.1 with Gurobi 9.0 (Gurobi 2022) and computed on a Windows 10 PC, Intel Xeon CPU E5-1620 3.60 GHz, and 32 GB of RAM.

5.1 Real-world instance data and preliminaries

We use the landscape and fire history data of Hawkesbury region in New South Wales, Australia, obtained from NSW Rural Fire Services (2016). This area covers 277,600 hectares, with about 28% privately owned, 69% managed by National Parks & Wildlife Services, and the remaining 3% managed by various other agencies. The graph representation of the area with 34 nodes and 71 edge is shown in Figure 3. We used the time-since-fire data to set t^{init} and x_i^1 (see Section EC.8 for details).

For fuel dynamics, we use the steady-state fuel load $L_i^{\max} = 16.4$ t/ha, annual decomposition rate $\kappa_i = 0.17$ with the corresponding inverse growth rate $\gamma_i = 0.84$, and minimum maturity $t_i^{\min} = 10$, consistent with the Hawkesbury's prevailing dry sclerophyll forest; see Watson (2011). The node activation threshold $L_i^{\text{thr}} = 13.4$ t/ha, treatment cost $c_i^t = 1$, and treatment budget (in number of areas) $b_t \in \{1,3,5\}$ were adopted from Matsypura et al. (2018). We set the treatment effectiveness parameter $\alpha = 0.51$, as suggested by Price et al. (2022).

To study our model's sensitivity to different levels of uncertainty, we use different values for the budget of uncertainty parameters $\beta_i^{t,\delta}$ and $\beta_i^{t,\eta}$. To simplify the exposition, we set $\beta_i^{t,\delta} = \hat{\beta}^{\delta}$ and $\beta_i^{t,\eta} = \hat{\beta}^{\eta}$ (i.e., the sames for all i and t), where $\hat{\beta}^{\delta}$ and $\hat{\beta}^{\eta}$ take different values for different experiments; specifically, $\hat{\beta}^{\delta}, \hat{\beta}^{\eta} \in \{0, 0.01, 0.02, 0.05\}$. Our choice of values for $\hat{\beta}^{\eta}$ is based on the measurements of $L^{\max}$ from the literature (Watson 2011, Bowman et al. 2021). A typical value for $L^{\max}$ in dry sclerophyll forests of the Hawkesbury area is 16.4 t/ha, with some regions reaching up to 18 t/ha. We selected the maximum value for $\hat{\beta}^{\eta}$ to be 0.05 because it corresponds to $L^{\max} \approx 18.0$ in our framework, depending on the initial fuel load (see Figure 2). The rest of the values of $\hat{\beta}^{\eta}$ were chosen to represent less extreme scenarios, with $\hat{\beta}^{\eta} = 0$ representing the absence of uncertainty. This range $\hat{\beta}^{\delta}$ also covers the necessary range of values for treatment effectiveness parameter α (Price et al. 2022).

To conduct the analysis, we compute the *mismatch loss*, which is analogous to the *mismatch cost* used widely in the Newsvendor Problem literature; see for example Olivares et al. (2008). Since no money is involved, we use the term *loss* instead of *cost* to avoid confusion. This loss reflects the reduction in policy performance due to the mismatch between the selected uncertainty level $\hat{\beta}^{\delta}, \hat{\beta}^{\eta}$ and the nature's ex post uncertainty level $\beta^{\delta}, \beta^{\eta}$. Hence, it tells us how much better we could have done if we had known the true values of β^{δ} and β^{η}. To describe the mismatch loss precisely, we introduce

the notation $(\mathbf{x}(\hat{\beta}^\delta, \hat{\beta}^\eta), \mathbf{z}(\hat{\beta}^\delta, \hat{\beta}^\eta))$ to denote the policy obtained by solving the corresponding version of **BDM**, **IRM** (for the fuel load objective) or **CRM** (for the active edges objective), for a given uncertainty level β^δ, β^η. We compute the mismatch loss for each combination of objective function and parameter values by repeating the following steps:

1. Pick an objective function (either total fuel load or number of active edges), a time horizon T, a treatment budget b_t, and a level of uncertainty $\hat{\beta}^\delta, \hat{\beta}^\eta$.
2. Compute the corresponding optimal policy $(\mathbf{x}(\hat{\beta}^\delta, \hat{\beta}^\eta), \mathbf{z}(\hat{\beta}^\delta, \hat{\beta}^\eta))$ by solving **BDM**, **IRM** or **CRM**, depending on which objective function and uncertainty level are selected in step 1.
3. Pick a "true" level of uncertainty β^δ, β^η and compute the corresponding evaluation function $\hat{v}(\hat{\beta}^\delta, \hat{\beta}^\eta; \beta^\delta, \beta^\eta) := f^{\text{IRM}}(\mathbf{x}(\hat{\beta}^\delta, \hat{\beta}^\eta), \mathbf{z}(\hat{\beta}^\delta, \hat{\beta}^\eta); \beta^\delta, \beta^\eta)$, e.g., by solving (19) for the fuel load objective, or (24) for the number of active edges objective.
4. Compute the "oracle" policy by setting $(\hat{\beta}^\delta, \hat{\beta}^\eta) = (\beta^\delta, \beta^\eta)$ and solving problem **BDM**, **IRM** or **CRM**, depending on which objective is selected in step 1.
5. Compute the corresponding oracle evaluation function $v^*(\beta^\delta, \beta^\eta) := f^{\text{IRM}}(\mathbf{x}(\beta^\delta, \beta^\eta), \mathbf{z}(\beta^\delta, \beta^\eta); \beta^\delta, \beta^\eta)$ for the policy obtained in step 4.
6. Compute the *mismatch loss* by taking the relative difference (as a percentage) between the two evaluation functions:

$$\text{MML}\left(\hat{\beta}^\delta, \hat{\beta}^\eta; \beta^\delta, \beta^\eta\right) := \left(\frac{\hat{v}(\hat{\beta}^\delta, \hat{\beta}^\eta; \beta^\delta, \beta^\eta) - v^*(\beta^\delta, \beta^\eta)}{v^*(\beta^\delta, \beta^\eta)} \times 100\right)\%. \tag{25}$$

5.2 Case study results and insights

There are four possible values for $\hat{\beta}^\delta$ and $\hat{\beta}^\eta$: $0, 0.01, 0.02, 0.05$, and three different budget thresholds, $b_t = 1, 3, 5$. This setting means that we computed 48 different policies for each objective function. We evaluated each policy using 16 combinations for β^δ and β^η over the same four values. In total, for each objective function, we performed 768 MML computations.

Figures 5 and 6 present the average MML over different budgets b_t, for selected pairs $\hat{\beta}^\delta$ and $\hat{\beta}^\eta$, while Figure 7 presents this values for different policies in the deterministic setting, and Figures 8 and 9 disaggregate the cases in Figures 5 and 6 for individual budgets. These combinations of $\hat{\beta}^\delta$, $\hat{\beta}^\eta$, β^δ and β^η best illustrate our findings, relegating the other combinations to Section EC.9 of the E-Companion. Our key findings are grounded in four questions.

Q1: *Do robust policies result in lower MML compared to non-robust ones?*

A1: Based on our study, there is evidence that utilizing robust models can benefit performance. For example, Figure 5(a) plots MML for total fuel load when there is *no* robustness in the model $(\hat{\beta}^\delta, \hat{\beta}^\eta) = (0, 0)$. Comparing this to Figure 5(c) we see that the MML is reduced for all combinations

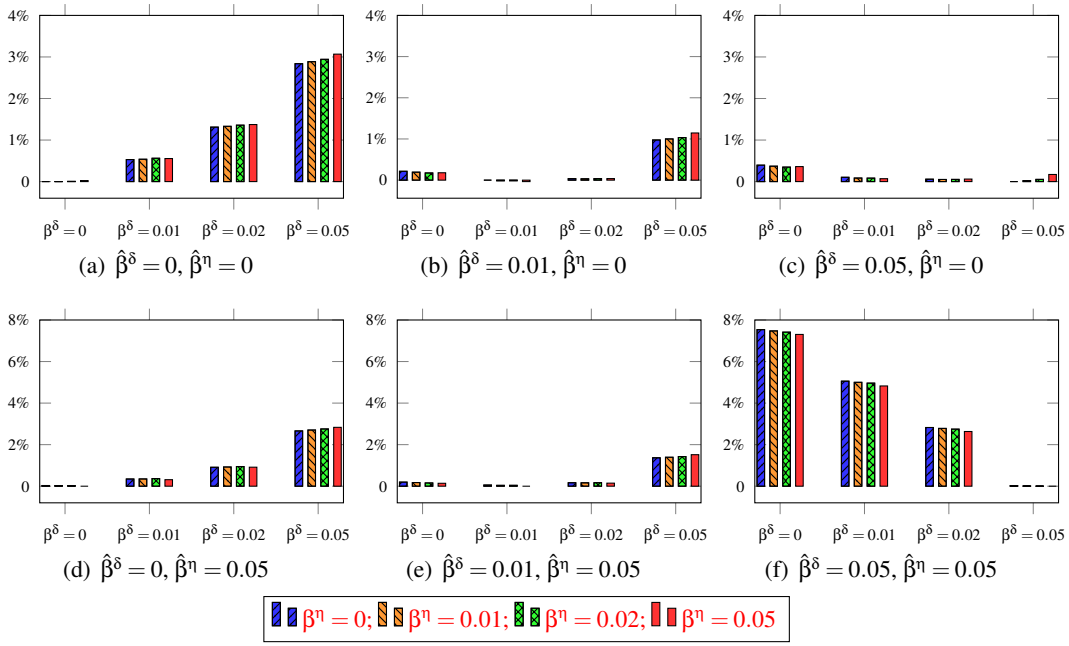

Figure 5 MML (mismatch loss) values for the total fuel load objective, averaged over different budgets $b_t = 1, 3, 5$.

of true parameters $(\beta^\delta, \beta^\eta)$ except for $(\beta^\delta, \beta^\eta) = (0, 0)$. The same comparison holds when comparing Figures 5(a) and 5(d). This observation means that for the total fuel load objective function, using a non-robust model is useful only when we have accurate estimates of the α, γ parameters. Otherwise, even a crude estimate of the magnitude of noise (i.e., $(\hat{\beta}^\delta, \hat{\beta}^\eta) = (0.05, 0)$ or $(\hat{\beta}^\delta, \hat{\beta}^\eta) = (0.01, 0.05)$) results in vastly reduced MML across a wide range of $(\beta^\delta, \beta^\eta)$. That said, we also see in Figure 5(f) that adding *too much* noise can be detrimental to performance. This observation also holds in Figure 6 for the number of active edges objective function. Compared to the policy obtained without any robustness (Figure 6(a)), the policy that performs most favorably is in Figure 6(b) when $(\hat{\beta}^\delta, \hat{\beta}^\eta) = (0.01, 0)$. In fact, across most parameter combinations, the MML in Figure 6(b) is lower than that in Figure 6(a). On the other hand, when we estimate larger amounts of uncertainty (e.g., $(\hat{\beta}^\delta, \hat{\beta}^\eta) = (0.05, 0.05)$), the performance of robust solutions can degrade for most combinations of $(\beta^\delta, \beta^\eta)$ except for those where our guess happens to be correct (see Figures 6(c) and 6(f)).

Insight I1: This observation suggests that planners who *do not* have a good sense of potential deviations in the estimated growth rate and treatment effectiveness parameters should introduce a *small* degree of robustness into the model. Even this small adjustment can improve performance compared to the non-robust model.

Q2: *Which uncertainty parameter affects MML the most?*

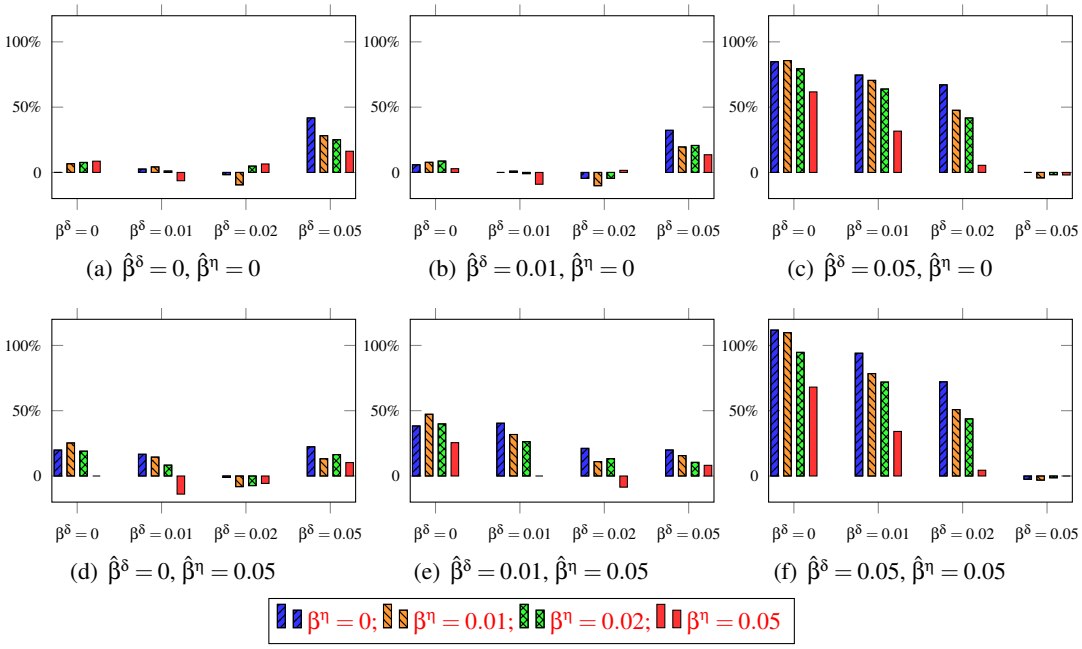

Figure 6 MML values for the number of active edges objective, averaged over different budgets $b_t = 1, 3, 5$.

A2: We find evidence that β^δ affects MML more than β^η for the total fuel load objective, which is strikingly seen in Figure 5. The different colored bars show different values of β^η. We see that when β^δ is held constant (within a group of four different colored bars), there is almost no change in the MML. On the other hand, when we compare different β^δ (groups of four bars), there is visible change in the MML. For the number of active edges, the conclusion is less clear, though there are some glimpses that this pattern holds here as well.

To make comparisons easier, we define and compute a measure of variation as follows. For each $\hat{\beta}^\delta, \hat{\beta}^\eta$ combination, we fix β^δ and compute the standard deviation of the four MML values from the different values of β^η. Since there are 16 combinations of $\hat{\beta}^\delta, \hat{\beta}^\eta$ and four values of β^δ, this gives us 64 different standard deviation computations. We then take the average of these 64 numbers, and denote it $\mathbf{std}(\delta)$. We repeat this but switch the role of β^δ and β^η, to get $\mathbf{std}(\eta)$. We obtain Table 1, which indeed shows that MML is more sensitive to β^δ.

Objective	$\mathbf{std}(\delta)$	$\mathbf{std}(\eta)$
Total fuel load	1.03%	0.03%
Number of active edges	19.10%	9.53%

Table 1 Variation in β^δ vs β^δ; see **A2** for how this measure is defined.

Insight I2: For the planners aiming to minimize fuel load, a deep understanding of potential deviations in treatment effectiveness (understanding the magnitude of β^δ) can improve model performance

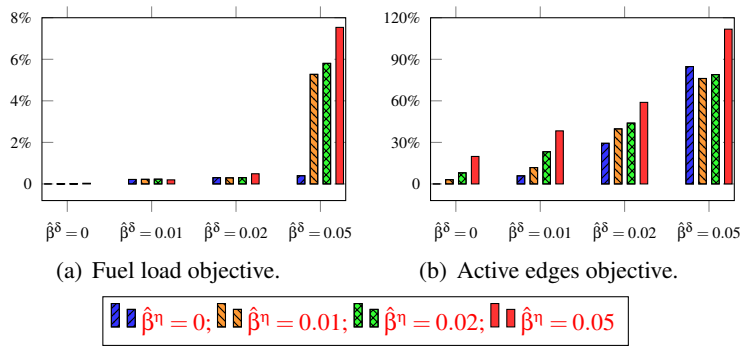

(a) Fuel load objective. (b) Active edges objective.

Figure 7 MML when there is no uncertainty (true: $\beta^{\eta}=\beta^{\delta}=0$); policy-design uncertainty budgets $(\hat{\beta}^{\eta},\hat{\beta}^{\delta})$ vary in $\{0,0.01,0.02,0.05\}$. Each bar is the average over three budgets $b_t=1,3,5$.

as it helps refine the choice of $\hat{\beta}^{\delta}$. On the other hand, model performance remains relatively consistent, regardless of the uncertainty in fuel growth (i.e., irrespective of the true value of β^{η}). Therefore, when planners have limited resources for gathering information and tuning model parameters, they should focus their efforts on more accurately estimating treatment effectiveness. If the planner aims to minimize the number of active edges, then this insight still holds, albeit to a lesser extent.

Q3: *What happens when estimated uncertainty levels* $(\hat{\beta}^{\eta},\hat{\beta}^{\delta})$ *are higher than the true levels* $(\beta^{\eta},\beta^{\delta})$*?*

A3: From the MML curves (see Figure 7) with true $\beta^{\eta}=\beta^{\delta}=0$, we obtain practical targets for the design of uncertainty levels $(\hat{\beta}^{\eta},\hat{\beta}^{\delta})$. For the *fuel-load* objective, lowering the treatment-effect uncertainty from high to moderate-high ($\hat{\beta}^{\delta}: 0.05 \to 0.02$) drives the loss close to the deterministic optimum even if $\hat{\beta}^{\eta}$ remains high. If fuel-growth noise is eliminated ($\hat{\beta}^{\eta}=0$), lowering uncertainty in treatment effect is unnecessary. For the *active-edges* objective, loss is large when either fuel growth and treatment effect uncertainty are high or moderate high, but decreases significantly once both are small ($\hat{\beta}^{\eta}=\hat{\beta}^{\delta}=0.01$).

Insight I3: A small level of robustness can ensure good performance even when there is no uncertainty.

Q4: *How does the size of the treatment budget affect MML?*.

A4: We find evidence that MML tends to increase with the rise in the treatment budget; see Figures 8 and 9. This observation is expected, as larger budgets allow for more treatments to be performed in each time period. This tendency is particularly pronounced for the number of active edges objective. When comparing the plots in Figure 9 from left to right, we observe a significant increase in the heights of the bars, especially in cases with high uncertainty in treatment effectiveness (i.e.,

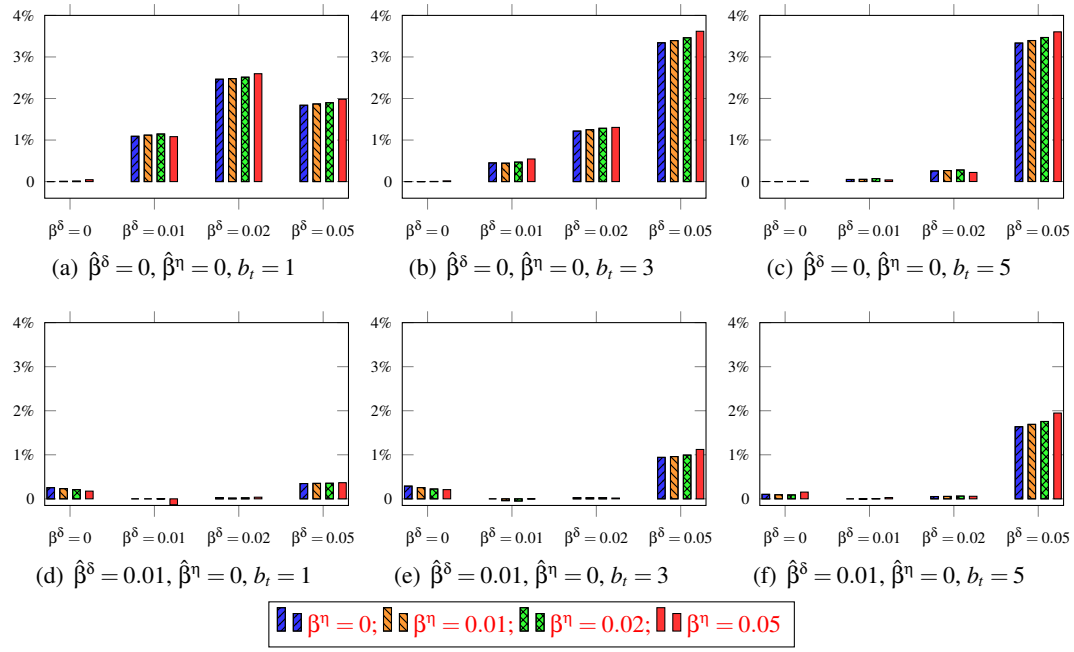

Figure 8 MML (mismatch loss) values of different budgets b_t, for the total fuel load objective.

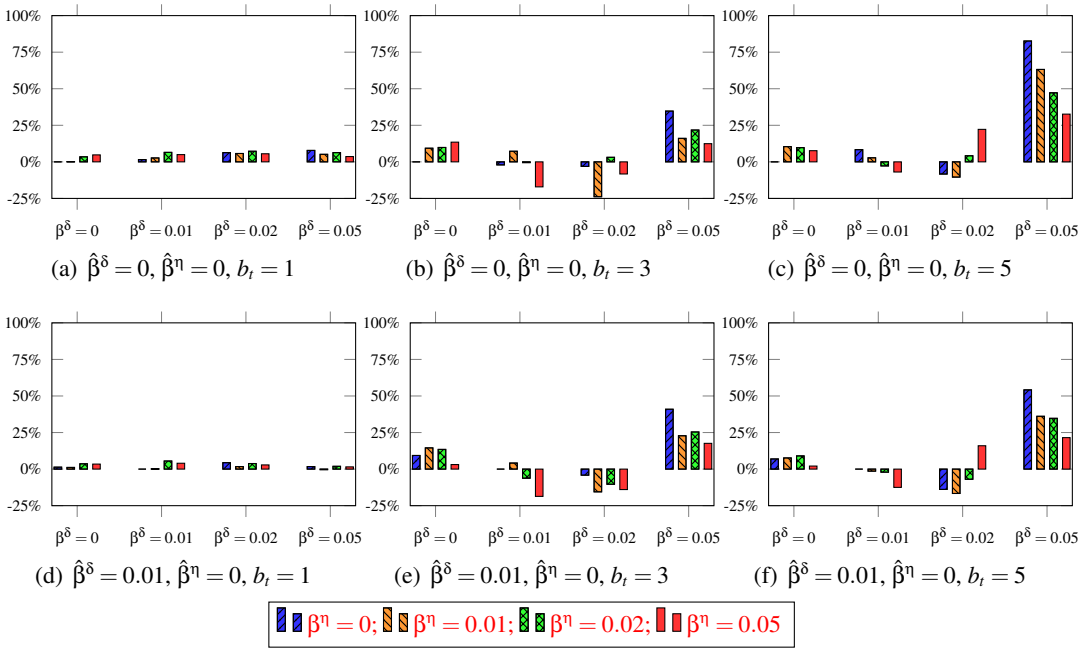

Figure 9 MML values of different budgets b_t, for the number of active edges objective.

$\beta^\delta = 0.05$). However, by comparing the top row of plots in Figure 9 with the corresponding plots in the bottom row, we see that using our robust model with a very modest level of uncertainty in treatment effectiveness (i.e., $\hat{\beta}^\delta = 0.01$) helps reduce variability in MML, particularly in situations

with a large budget and nature's true uncertainty level (i.e., $b_t = 5$ and $\beta^\delta = 0.05$). We observe a similar pattern for the total fuel load objective, albeit on a smaller scale; see Figure 8. For example, by introducing small amount of robustness in treatment effectiveness, we reduce the corresponding MML three-fold and more for moderate budget case (Figures 8(b) and 8(e)) and about two-fold for the large budget case (Figures 8(c) and 8(f)).

Insight I4: Practitioners with larger treatment budgets should exercise extra caution when using fuel-based objectives to determine fuel treatment plans, since models are more susceptible to uncertainty. More importantly, robust optimization offers a cost-effective method to mitigate this vulnerability without having to expend resources in improving parameter estimates.

6 Conclusions

We develop a robust multi-period fuel treatment model that incorporates parameterized uncertainty in fuel growth and treatment effectiveness. In addition, our deterministic model can solve the problem presented in Matsypura et al. (2018) using fewer variables and constraints.

Through an experimental analysis utilizing data from dry sclerophyll forests in the Hawkesbury region, located in NSW, Australia, we derive practical insights. Our findings indicate that using a robust approach can mitigate losses due to higher uncertainty in fuel data, potentially resulting in minimal losses across different objectives when considering fuel load as an indicator of wildfire risk. Moreover, we demonstrate that in our real life study accurate estimation of fuel treatment effectiveness holds greater importance than estimation of fuel growth. Furthermore, under more intensive treatment, treatment effect estimation gains greater importance. Finally, we illustrate the differences in the solution structure between different objectives and levels of uncertainty and provide an explanation of the factors driving these differences.

Future work may explore the integration of additional fuel treatment planning aspects, such as incorporating high-value asset protection via more tailored objective functions. Another extension can consider modeling rate-of-spread using landscape and weather information.

References

Acuna, Mauricio A, Cristian D Palma, Wenbin Cui, David L Martell, Andres Weintraub. 2010. Integrated spatial fire and forest management planning. *Canadian Journal of Forest Research*, 40 (12), 2370-2383.

Bertsimas, Dimitris, Melvyn Sim. 2004. The price of robustness. *Operations Research*, 52 (1), 35-53.

Bertsimas, Dimitris, Aurlie Thiele. 2006. A robust optimization approach to inventory theory. *Oper. Res.*, 54 (1), 150–168.

Bhuiyan, Tanveer Hossain, Maxwell C Moseley, Hugh R Medal, Eghbal Rashidi, Robert K Grala. 2019. A stochastic programming model with endogenous uncertainty for incentivizing fuel reduction treatment under uncertain landowner behavior. *European Journal of Operational Research*, 277 (2), 699-718.

Bowman, David M.J.S., Grant J. Williamson, Owen F. Price, Mercy N. Ndalila, Ross A. Bradstock. 2021. Australian forests, megafires and the risk of dwindling carbon stocks. *Plant, Cell & Environment*, 44 (2), 347-355.

Charnley, Susan, Melissa R. Poe, Alan A. Ager, Thomas A. Spies, Emily K. Platt, Keith A. Olsen. 2015. A Burning Problem: Social Dynamics of Disaster Risk Reduction through Wildfire Mitigation. *Human Organization*, 74 (4), 329-340.

Ehsani, Mohammad Reza, Jorge Arevalo, Christoforus Bayu Risanto, Mostafa Javadian, Charles John Devine, Alireza Arabzadeh, Hector L. Venegas-Quiñones, Ambria Paige Dell'Oro, Ali Behrangi. 2020. 2019–2020 Australia fire and its relationship to hydroclimatological and vegetation variabilities. *Water*, 12 (11), 3067.

Finney, Mark A. 2001. Design of regular landscape fuel treatment patterns for modifying fire growth and behavior. *Forest Science*, 47 (2), 219-228.

Gillen, Colin P, Dmytro Matsypura, Oleg A Prokopyev. 2017. Operations research techniques in wildfire fuel management. *Optimization Methods and Applications*. Springer, Cham, Switzerland, 119-135.

Glover, Fred. 1975. Improved linear integer programming formulations of nonlinear integer problems. *Management Science*, 22 (4), 455-460.

Gupta, Sushil, Martin K. Starr, Reza Zanjirani Farahani, Niki Matinrad. 2016. Disaster management from a pom perspective: Mapping a new domain. *Production and Operations Management*, 25 (10), 1611-1637.

Gurobi. 2022. Gurobi Optimizer Reference Manual.

Hunter, Molly E., Michael H. Taylor. 2022. The economic value of fuel treatments: A review of the recent literature for fuel treatment planning. *Forests*, 13 (12),.

Hyndman, Rob, Anne Koehler, Keith Ord, Ralph Snyder. 2008. *Forecasting with Exponential Smoothing: The State Space Approach*. Springer, Berlin, Heidelberg. doi:10.1007/978-3-540-71918-2.

Igini, Martina. 2023. What causes wildfires? https://earth.org/what-causes-wildfires/, last accessed August 2024.

Kane, Jeffrey. 2025. Prescribed fire. https://www.britannica.com/science/prescribed-fire, last accessed September 2025.

Kenny, B, E Sutherland, E Tasker, B Bradstock. 2004. Guidelines for ecologically sustainable fire management. Technical report, NSW Biodiversity Strategy and NSW National Parks and Wildlife Service.

Lagos, Tomás, Junyeong Choi, Brittany Segundo, Jianbang Gan, Lewis Ntaimo, Oleg A. Prokopyev. 2025. Bilevel optimization approach for fuel treatment planning. *European Journal of Operational Research*, 320 (1), 205-218.

León, Javier, Begoña Vitoriano, John Hearne. 2023. A risk-averse solution for the prescribed burning problem. *Safety Science*, 158 105951.

Martell, David L. 2015. A review of recent forest and wildland fire management decision support systems research. *Current Forestry Reports*, 1 (2), 128-137.

Matsypura, Dmytro, Oleg A. Prokopyev, Aizat Zahar. 2018. Wildfire fuel management: Network-based models and optimization of prescribed burning. *European Journal of Operational Research*, 264 (2), 774 - 796.

McCaw, W. Lachlan. 2013. Managing forest fuels using prescribed fire – a perspective from southern Australia. *Forest Ecology and Management*, 294 217-224.

McCormick, Garth P. 1976. Computability of global solutions to factorable nonconvex programs: Part i — convex underestimating problems. *Mathematical Programming*, 10 (1), 147-175.

Minas, James, John Hearne, David Martell. 2013. An integrated optimization model for fuel management and fire suppression preparedness planning. *Annals of Operations Research*, 232 (1), 201-215.

Minas, James P, John W Hearne, David L Martell. 2014. A spatial optimisation model for multi-period landscape level fuel management to mitigate wildfire impacts. *European Journal of Operational Research*, 232 (2), 412-422.

Morgan, GW, KG Tolhurst, MW Poynter, N Cooper, T McGuffog, R Ryan, MA Wouters, N Stephens, P Black, D Sheehan, et al. 2020. Prescribed burning in south-eastern Australia: history and future directions.

Australian Forestry, 83 (1), 4-28.

NASA Earth Observatory. 2023. Tracking Canada's extreme 2023 fire season. https://earthobservatory.nasa.gov/images/151985/tracking-canadas-extreme-2023-fire-season, last accessed August 2024.

NIFC. 2022. National Interagency Fire Center, Federal Firefighting Costs. https://www.nifc.gov/fire-information/statistics/suppression-costs, last accessed August 2024.

Nohadani, Omid, Kartikey Sharma. 2018. Optimization under decision-dependent uncertainty. *SIAM Journal on Optimization*, 28 (2), 1773-1795.

NSW Rural Fire Services, Hawkesbury Bush Fire Management Committee. 2016. Fire history gis data set.

Olivares, Marcelo, Christian Terwiesch, Lydia Cassorla. 2008. Structural estimation of the newsvendor model: An application to reserving operating room time. *Management Science*, 54 (1), 41-55.

Olson, Jerry S. 1963. Energy storage and the balance of producers and decomposers in ecological systems. *Ecology*, 44 (2), 322-331.

Poss, Michael. 2013. Robust combinatorial optimization with variable budgeted uncertainty. *4OR*, 11 75-92.

Price, Owen F., Ross A. Bradstock. 2012. The efficacy of fuel treatment in mitigating property loss during wildfires: Insights from analysis of the severity of the catastrophic fires in 2009 in victoria, australia. *Journal of Environmental Management*, 113 146-157.

Price, Owen H., Rachael H. Nolan, Stephanie A. Samson. 2022. Fuel consumption rates in resprouting eucalypt forest during hazard reduction burns, cultural burns and wildfires. *Forest Ecology and Management*, 505 119894.

Rachmawati, Ramya, Melih Ozlen, John Hearne, Karin Reinke. 2018. Fuel treatment planning: Fragmenting high fuel load areas while maintaining availability and connectivity of faunal habitat. *Applied Mathematical Modelling*, 54 298-310.

Rachmawati, Ramya, Melih Ozlen, Karin J. Reinke, John W. Hearne. 2015. A model for solving the prescribed burn planning problem. *SpringerPlus*, 4 (1), 630.

Rachmawati, Ramya, Melih Ozlen, Karin J. Reinke, John W. Hearne. 2016. An optimisation approach for fuel treatment planning to break the connectivity of high-risk regions. *Forest Ecology and Management*, 368 94 - 104.

Troncoso, Juan J., Andrés Weintraub, David L. Martell. 2016. Development of a threat index to manage timber production on flammable forest landscapes subject to spatial harvest constraints. *INFOR: Information Systems and Operational Research*, 54 (3), 262-281.

U.S. Environmental Protection Agency. 2024. Wildfires. https://www.epa.gov/natural-disasters/wildfires, last accessed August 2024.

Watson, P. 2011. Fuel load dynamics in nsw vegetation–part 1: forests and grassy woodlands.

Wei, Yu. 2012. Optimize landscape fuel treatment locations to create control opportunities for future fires. *Canadian Journal of Forest Research*, 42 (6), 1002-1014.

Wei, Yu, Yehan Long. 2014. Schedule fuel treatments to fragment high fire hazard fuel patches. *Mathematical & Computational Forestry & Natural Resource Sciences*, 6 (1), 1.

Wei, Yu, Douglas Rideout, Andy Kirsch. 2008. An optimization model for locating fuel treatments across a landscape to reduce expected fire losses. *Canadian Journal of Forest Research*, 38 (4), 868-877.

World Health Organization. 2024. Wildfires. https://www.who.int/health-topics/wildfires, last accessed August 2024.

Yemshanov, Denys, Ning Liu, Daniel K Thompson, Marc-André Parisien, Quinn E Barber, Frank H Koch, Jonathan Reimer. 2021. Detecting critical nodes in forest landscape networks to reduce wildfire spread. *PloS one*, 16 (10), e0258060.

Zazali, Hilyati H, Isaac N Towers, Jason J Sharples. 2021. A critical review of fuel accumulation models used in australian fire management. *International journal of wildland fire*, 30 (1), 42-56.

E-Companion for Robust Network-based Optimization for Multi-Period Fuel Treatment Planning

Contents

EC.1 Nomenclature **ec2**

EC.2 Summary of the size complexity of the models **ec3**

EC.3 Derivation of the noisy fuel load dynamics in the absence of treatment **ec3**

EC.4 Linearizing noisy fuel dynamics **ec4**

EC.5 Example of (13) and the proof of Proposition 1 **ec8**

EC.6 Robust Mixed Integer Reformulation of Conservative Approximation **ec8**

EC.7 Reformulation ideal robust model total fuel load minimization **ec10**

EC.8 Initial maturities **ec11**

EC.9 Additional computational results **ec11**

EC.9.1 Additional robust policies and optimization results in Hawkesbury ec11

EC.9.2 Random instances generation ec14

EC.9.3 Scalability study random instances ec14

EC.1 Nomenclature

Sets and Parameters			
V	Set of fuel treatments areas, $\lvert V\rvert = n$	$b^t \in \mathbb{R}_+$	total budget available for treatment at time t
$E \subseteq V \times V$	Set of tuples of areas, representing their adjacency	$t_i^{\text{init}} \in \mathbb{Z}_+$	Initial age of a patch of area (number of periods since last fire or treatment)
$T \in \mathbb{Z}_+$	Number of time periods planning horizon, $[T] := \{1, \dots, T\}$	$t_i^{\min} \in \mathbb{Z}_+$	Minimum time required for maturity of vegetation species
$L_i^{\max} \geq 0$	Steady-state fuel load	$t_i^{\text{start}} =$	$\max\{t_i^{\min} - t_i^{\text{init}}, 0\}$
$L^{\text{init}} \geq 0$	initial fuel load after the most recent fire	$\beta_i^{t,\delta}, \beta_i^{t,\eta} \geq 0$	Protection level increment at time t in $\Gamma_i^{t,\delta}(\mathbf{z}_i)$ and $\Gamma_i^{t,\eta}(\mathbf{z}_i)$, respectively, if treatment is not performed
$L \geq 0$	mean annual surface fuel that accumulates	$\beta_{\text{opt}}^{\delta}, \beta_{\text{opt}}^{\eta} \geq 0$	Protection level increment $\beta_i^{t,\delta} = \beta_{\text{opt}}^{\delta}$ and $\beta_i^{t,\eta} = \beta_{\text{opt}}^{\eta}$, respectively, for policy computation
$\alpha_i \in [0,1]$	Remaining fraction of accumulated fuel load one period after treatment	$\beta_{\text{eval}}^{\delta}, \beta_{\text{eval}}^{\eta} \geq 0$	Protection level increment $\beta_i^{t,\delta} = \beta_{\text{eval}}^{\delta}$ and $\beta_i^{t,\eta} = \beta_{\text{eval}}^{\eta}$, respectively, for policy evaluation
$\kappa_i \in [0,1]$	Decomposition rate of forest litter	$\Gamma_i^{0,\delta}, \Gamma_i^{0,\eta} \geq 0$	Nature's initial budget for fuel load noise allocation
$\gamma_i \in [0,1]$	Inverse growth rate	$L_i^{\text{thr}} \geq 0$	Fuel load threshold for node activation
$c_i^t \in \mathbb{R}_+$	cost of treating area i at time t		
Variables			
$x_i^t \geq 0$	Deterministic fuel load, $\mathbf{x} = (x_i^t)_{i \in V, t \in [T+1]}$	$z_i^t \in \{0,1\}$	Fuel treatment decision variable, $\mathbf{z}_i = (z_i^t)_{t \in [T]}$, $\mathbf{z} = (z_i^t)_{i \in V, t \in [T]}$
$\tilde{\delta}_i^t, \tilde{\eta}_i^t \in [0,1]$	Relative increase in fuel load parameters by nature in the idea setting, $\tilde{\delta}_i^{[t]} = (\tilde{\delta}_i^s)_{s \in [t]}$, $\tilde{\eta}_i^{[t]} = (\tilde{\eta}_i^s)_{s \in [t]}$	$\delta_i^{t,s}, \eta_i^{t,s} \in [0,1]$	Relative increase in fuel load parameters by nature in the conservative setting, $\delta_i^{t,[t]} = (\delta_i^{t,s})_{s \in [t]}$, $\eta_i^{t,[t]} = (\eta_i^{t,s})_{s \in [t]}$
$\tilde{y}_i^t \geq 0$	Fuel load noise in the ideal setting, $\tilde{\mathbf{y}} = (\tilde{y}_i^t)_{i \in V, t \in [T+1]}$	$\tilde{x}_i^t \geq 0$	Total (deterministic plus noise) fuel load curve
$y_i^t \geq 0$	Fuel load noise in the conservative setting, $\mathbf{y} = (y_i^t)_{i \in V, t \in [T+1]}$	$\omega_i^t, \sigma_i^t \geq 0$	Dual variables associated with nature's surge allocation budget constraints
$\tilde{\xi}_i^t, \tilde{\zeta}_i^t \geq 0$	Dual variable associated with $\tilde{\delta}_i^t, \tilde{\eta}_i^t \leq 1$	$\xi_i^{t,s}, \zeta_i^{t,s} \geq 0$	Dual variable associated with $\delta_i^{t,s}, \eta_i^{t,s} \leq 1$
$v_{i,t}^{s,k} \in \{0,1\}$	Variable indicating whether number of treatments in area i in periods $s, \dots, t$ is equal to $k \in \{0, \dots, t-s\}$, $\mathbf{v}_{i,t} = (v_{i,t}^{s,k})_{s \in [t], k \in \{0,\dots,t-s\}}$	$\phi_{i,j}^t \in \{0,1\}$	Variable indicating whether both areas $i, j \in V$, at time t, belong to the same connected components in the graph induced by active edges
$\theta_i^t \in \{0,1\}$	Variable indicating whether the cell is active	$\varepsilon_{i,j}^t$	Variable indicating whether $\theta_i^t = \theta_j^t = 1$, for $i, j \in V$
$\rho_i^t \in \{0,1\}$	Variable indicating whether area i has the largest index in its connected component	$\mu_{i^*,j^*}^{i,j,t} \geq 0$	$t \in [T+1]$, $(i,j) \in V^2 \setminus E \colon i < j$, $(i^*, j^*) \in E$
$\pi_{i,t}^{s,k} =$	$v_{i,t}^{s,k}(1 - z_i^s)$	$u_i^t =$	$z_i^t x_i^t$
$\chi_{i,t}^{s,k} =$	$v_{i,t}^{s,k} u_i^t$	$\lambda_i^{t,s} =$	$(1 - z_i^s)(\omega_i^t + \sigma_i^t)$
$\Gamma_i^{t,\delta}(\mathbf{z}_i), \Gamma_i^{t,\eta}(\mathbf{z}_i) \geq 0$	Nature's uncertainty budgets for noise allocation		

Table EC.1 Definitions of sets, parameters, and variables.

EC.2 Summary of the size complexity of the models

		System		# of variables	# of constraints
Base		Matsypura et al. (2018)		$O(nT^2)$	$O(nT^3)$
		BDM		$O(nT)$	$O(nT)$
		BNM		$O(nT^3/t^{\min})$	$O(nT^3/t^{\min})$
		IRM	**UP:**	$O(nT^3/t^{\min})$	$O(nT^3/t^{\min})$
			LL:	$O(nT)$	$O(nT)$
		CRM	**UP:**	$O(nT^3/t^{\min})$	$O(nT^3/t^{\min})$
			LL:	$O(nT^2)$	$O(nT^2)$
		CRM (single-level reformulation)		$O(nT^3/t^{\min})$	$O(nT^3/t^{\min})$
		RMIP (after linearizations EC.4, EC.6)		$O(nT^3/t^{\min})$	$O(nT^3/t^{\min})$
Objectives	Planner	(18) (Fuel load)		$O(nT)$	$O(nT)$
		(22) (Active edges)		$O((\|E\|+n)T)$	$O((\|E\|+n)T)$
	Nature	(19) (Fuel load)		$O(nT)$	$O(nT)$
		(24) (Active edges)		$O((\|E\|+n)T)$	$O((\|E\|+n)T)$
Solved Formulations	Matsypura et al. (2018)+	(18)		$O(nT^2)$	$O(nT^3)$
		(22)		$O(\|E\|T+nT^2)$	$O(\|E\|T+nT^3)$
	BDM+	(18)		$O(nT)$	$O(nT)$
		(22)		$O((\|E\|+n)T)$	$O((\|E\|+n)T)$
	IRM+	(18) = (EC.10)		$O(nT^3/t^{\min})$	$O(nT^3/t^{\min})$
	RMIP+	(22)		$O(nT^3/t^{\min}+\|E\|T)$	$O(nT^3/t^{\min}+\|E\|T)$

Table EC.2 Size complexity in terms of number of variables and number of constraints of the different models considered in this work. The base models size complexities are calculated considering that the modeling of f is dominated by the other components of the model. Each of the planner objectives can be combined with the base models, whereas the nature objectives are used to assess the value of a given policy in the **IRM** setting. Finally, for the solved formulations size complexities result from the different combinations of base models and planner's objectives that we use to compute treatment plans. We also include the size complexity of the formulation from Matsypura et al. (2018) for comparison.

EC.3 Derivation of the noisy fuel load dynamics in the absence of treatment

In this section we derive the expression used in (6). Recall that the noisy fuel load are given by

$$\tilde{x}^{t+1} = \gamma \tilde{x}^t + (1-\gamma)\overline{L}^{\max}(t), \tag{EC.1}$$

and that $\overline{L}^{\max}(t) = (1+\tilde{\eta}^t)L^{\max}$. Hence, it follows that:

$$\begin{aligned}
\tilde{x}^{t+1} &= \gamma \tilde{x}^t + (1-\gamma)\overline{L}^{\max}(t) \\
&= \gamma \tilde{x}^t + (1-\gamma)L^{\max}(1+\tilde{\eta}^t) \\
&= \gamma^2 \tilde{x}^{t-1} + (1-\gamma)L^{\max}(\gamma(1+\tilde{\eta}^{t-1}) + (1+\tilde{\eta}^t)) \\
&\vdots \\
&= \gamma^{t+1} L^{\text{init}} + (1-\gamma)L^{\max} \sum_{s\in[t]} \gamma^{t-s}(1+\tilde{\eta}^s) \\
&= \gamma^{t+1} L^{\text{init}} + L^{\max}(1-\gamma^{t+1}) + (1-\gamma)L^{\max} \sum_{s\in[t]} \gamma^{t-s}\tilde{\eta}^s
\end{aligned}$$

$$
\begin{aligned}
&= x^{t+1} + (1-\gamma) L^{\max} \sum_{s\in[t]} \gamma^{t-s} \tilde{\eta}^s \\
&= x^{t+1} + \gamma(\tilde{x}^t - x^t) + (1-\gamma) L^{\max} \tilde{\eta}^t. \qquad (6)
\end{aligned}
$$

The first four equalities are obtained by applying (EC.1) iteratively. The fifth equality follows from the fact that $(1-\gamma^t) = (1-\gamma)\sum_{s\in[t]} \gamma^{t-s}$. The sixth equality follows from the definition of x^{t+1}, and the last equality is derived by substituting the obtained expression for $\tilde{x}^t$.

REMARK EC.1. *Upper bound of the fuel accumulation function as $t = T \to \infty$ in an area not treated.* Clearly, Olson's curve (2) is bounded above by $L^{\max}$, hence $x^\infty \le L^{\max}$. Next, from the derivation of (6), we have

$$
\tilde{x}^\infty = x^\infty + (1-\gamma) L^{\max} \lim_{T\to\infty} \sum_{s\in[T]} \gamma^{T-s} \tilde{\eta}^s \le L^{\max} + L^{\max}(1-\gamma) \sum_{s=0}^{\infty} \gamma^s = 2L^{\max},
$$

where the inequality follows from $\tilde{\eta}^s \le 1$. Since $x^\infty \to L^{\max}$, this implies that the total amount of noise is bounded by $L^{\max}$. This observation allows us to construct useful objective measures in Section 4. □

EC.4 Linearizing noisy fuel dynamics

In this section, we linearize the expression

$$
\tilde{y}_i^{t+1} = \sum_{s=1}^{t} \gamma_i^{\sum_{\tau=s+1}^{t} 1-z_i^\tau} \left((1-\alpha_i) \tilde{\delta}_i^s x_i^s z_i^s + (1-\gamma_i) L_i^{\max} \tilde{\eta}_i^s (1-z_i^s) \right), \qquad (10)
$$

by using the binary variable

$$
v_{i,t}^{s,k} = \begin{cases} 1, & \text{if } \sum_{\tau=s+1}^{t} (1-z_i^\tau) = k \\ 0, & \text{otherwise.} \end{cases} \qquad (v\text{-def})
$$

From this definition, (10) becomes

$$
\tilde{y}_i^{t+1} = \sum_{s=1}^{t} \left(\left((1-\alpha_i) \tilde{\delta}_i^s x_i^s z_i^s + (1-\gamma_i) L_i^{\max} \tilde{\eta}_i^s (1-z_i^s) \right) \sum_{k=0}^{t-s} \gamma_i^k v_{i,t}^{s,k} \right), \quad \forall i \in V,\ t \in [T]. \qquad (\text{Noise})
$$

Note that constraints (v-def) and (Noise) are still nonlinear, but they are a lot easier to deal with than constraint (10). In particular, (Noise) contains only bilinear terms, at one of which involves binary variables, thus can be linearized using the standard Glover's technique; see Glover (1975), McCormick (1976). Thus, to linearize (v-def), we first show that it is equivalent to the following set of bilinear equations involving z:

$$
\begin{aligned}
& v_{i,t}^{t,0} = 1, && \forall i \in V,\ t \in [T], && \text{(EC.2a)} \\
& v_{i,t}^{s,0} = v_{i,t}^{s+1,0} z_i^{s+1}, && \forall i \in V,\ t \in [T],\ s \in [t-1], && \text{(EC.2b)} \\
& v_{i,t}^{s,k} = v_{i,t}^{s+1,k-1} (1-z_i^{s+1}) + v_{i,t}^{s+1,k} z_i^{s+1}, && \forall i \in V,\ t \in [T],\ s \in [t-2],\ k \in [t-s-1], && \text{(EC.2c)}
\end{aligned}
$$

$$v_{i,t}^{s,t-s} = v_{i,t}^{s+1,t-s-1}(1-z_i^{s+1}), \qquad \forall i \in V,\, t \in [T],\, s \in [t-1]. \tag{EC.2d}$$

Here, (EC.2a) reflects the initial condition that $\sum_{s=t+1}^{t}(1-z_i^s)=0$ is always true. The following three sets of constraints reflect the fact that in each period for a given cell i, the number of treatments can either stay the same or increase by a maximum of one. First, (EC.2b) imposes that $v_{i,t}^{s,0}=1$ if and only if treatments are done every period between $s+2$ and t (i.e., $v_{i,t}^{s+1,0}=1$) and treatment is also done at time period $s+1$ (i.e., $z_i^{s+1}=1$). Then, in (EC.2c) $v_{i,t}^{s,k}$ can take the value of 1 if and only if either there are $t-s-k$ treatments performed in cell i in the time interval $[s+2,t]$ (i.e., $v_{i,t}^{s+1,k-1}=1$) and no treatment is done at time $s+1$ (i.e., $z_i^{s+1}=0$), or there are $t-s-k-1$ treatments in the interval $[s+2,t]$ (i.e., $v_{i,t}^{s+1,k}=1$) and treatment is done at time $s+1$ (i.e., $z_i^{s+1}=1$). Finally, (EC.2d) ensures that $v_{i,t}^{s,t-s}=1$ if and only if no treatment is done in the range $[s+2,t]$ (i.e., $v_{i,t}^{s+1,t-s-1}=1$) and no treatment is done at time $s+1$ (i.e., $z_i^{s+1}=0$). Note that non-negativity constraints on $\mathbf{v}=(v_{i,t}^{s,k})_{i\in V,t\in[T],s\in[t],k\in\{0,\ldots,t-s\}}$ are implicit due to (EC.2a) and non-negativity of $\mathbf{z}=(z_i^t)_{i\in V,t\in[T]}$.

Next, we present a result that shows the validity of our modeling of (*v*-def) using (EC.2).

PROPOSITION EC.1. *Suppose that $z_i^t \in \{0,1\}$ for all $i \in V$ and $t \in [T]$ holds. If $\mathbf{v}$ satisfies (EC.2), then $v_{i,t}^{s,k}$ satisfies (v-def), for all $i \in V$, $t \in [T]$, $s \in [t]$ and $k \in \{0,\ldots,t-s\}$.*

Proof. Let $z_i^t \in \{0,1\}$ for all $i \in V$ and $t \in [T]$. We aim to model $v_{i,t}^{s,k}=1 \iff \sum_{\tau=s+1}^{t}(1-z_i^\tau)=k$ for all $k \in \{0,1,\ldots,t-s\}$ and $s \in [t]$. For $s=t$, we clearly have $\sum_{\tau=s+1}^{t}(1-z_i^\tau)=0$ hence $v_{i,t}^{t,0}=1$ always. For $s=t-1$, we have $\sum_{\tau=s+1}^{t}(1-z_i^\tau)=1-z_i^t$, which verifies $v_{i,t}^{t-1,0}=v_{i,t}^{t,0}z_i^t$ in (EC.2b) and $v_{i,t}^{t-1,1}=v_{i,t}^{t,0}(1-z_i^t)$ in (EC.2d).

Now assume that for some $s \in [t-2]$ we know $v_{i,t}^{s+1,k'}=1 \iff \sum_{\tau=s+2}^{t}(1-z_i^\tau)=k'$ for all $k' \in \{0,\ldots,t-s-1\}$. We now show that this implies that $v_{i,t}^{s,k'}=1 \iff \sum_{\tau=s+1}^{t}(1-z_i^\tau)=k'$ for all $k' \in \{0,\ldots,t-s\}$. Consider $\sum_{\tau=s+1}^{t}(1-z_i^\tau)=(1-z_i^{s+1})+\sum_{\tau=s+2}^{t}(1-z_i^\tau)$. We break the analysis down into the following cases:

- $\sum_{\tau=s+2}^{t}(1-z_i^\tau)=0$. By our inductive hypothesis we have $v_{i,t}^{s+1,0}=1$ and all other $v_{i,t}^{s+1,k}=0$ for $k \in [t-s-1]$, hence by (EC.2):

$$v_{i,t}^{s,0} = z_i^{s+1}, \text{ by (EC.2b)},$$
$$v_{i,t}^{s,1} = 1-z_i^{s+1}, \text{ by (EC.2c)},$$

  with $v_{i,t}^{s,k}=0$ for all other $k \in \{2,\ldots,t-s\}$, implied by (EC.2c) and (EC.2d). Thus, we deduce:
  — If $z_i^{s+1}=1$ then $\sum_{\tau=s+1}^{t}(1-z_i^\tau)=1-z_i^{s+1}=0$, and we have $v_{i,t}^{s,0}=1$.
  — If $z_i^{s+1}=0$ then $\sum_{\tau=s+1}^{t}(1-z_i^\tau)=1-z_i^{s+1}=1$, and we have $v_{i,t}^{s,1}=1$.

- $\sum_{\tau=s+2}^{t}(1-z_i^\tau)=k$, for some $k\in[t-s-1]$. Then, by induction, $v_{i,t}^{s+1,k}=1$ and all other $v_{i,t}^{s+1,k'}=0$ for $k'\in[t-s]\setminus\{k\}$, consequently system (EC.2) implies:

$$v_{i,t}^{k,s}=z_i^{s+1} \quad \text{and} \quad v_{i,t}^{s,k+1}=1-z_i^{s+1}, \text{ by (EC.2c)},$$

with $v_{i,t}^{s,k'}=0$ for all other $k'\in\{0,\dots,t-s\}\setminus\{k,k+1\}$, by (EC.2b), (EC.2c) and (EC.2d). Now we have established that:

—If $z_i^{s+1}=1$ then $\sum_{\tau=s+1}^{t}(1-z_i^\tau)=k+1-z_i^{s+1}=k$, and we have $v_{i,t}^{s,k}=1$.

—If $z_i^{s+1}=0$ then $\sum_{\tau=s+1}^{t}(1-z_i^\tau)=k+1-z_i^{s+1}=k+1$, and we have $v_{i,t}^{s,k+1}=1$.

- $\sum_{\tau=s+2}^{t}(1-z_i^\tau)=t-s-1$. Then, again by the inductive hypothesis, $v_{i,t}^{s+1,t-s-1}=1$, and for all $k\in[t-s-2]$ $v_{i,t}^{s+1,k}=0$, hence from bilinear system (EC.2) we get:

$$v_{i,t}^{s,t-s-1}=z_i^{s+1}, \text{ by (EC.2c)},$$
$$v_{i,t}^{s,t-s}=1-z_i^{s+1}, \text{ by (EC.2d)},$$

with $v_{i,t}^{s,k'}=0$ for all $k'\in\{0,\dots,t-s-2\}$, by (EC.2b) and (EC.2c). Therefore, we conclude:

—If $z_i^{s+1}=1$ then $\sum_{\tau=s+1}^{t}(1-z_i^\tau)=t-s-1+1-z_i^{s+1}=t-s-1$, and we have $v_{i,t}^{s,t-s-1}=1$.

—If $z_i^{s+1}=0$ then $\sum_{\tau=s+1}^{t}(1-z_i^\tau)=t-s-1+1-z_i^{s+1}=t-s$, and we have $v_{i,t}^{s,t-s}=1$.

■

Next, we use the standard linearization technique to tackle the non-linear terms in (EC.2); see (Glover 1975, McCormick 1976). A linearized version of (EC.2) is presented next (note that it should include (EC.2a) to be complete).

$$\begin{aligned} &v_{i,t}^{s,0}\geq v_{i,t}^{s+1,0}+z_i^{s+1}-1,\\ &v_{i,t}^{s,0}\leq v_{i,t}^{s+1,0},\\ &v_{i,t}^{s,0}\leq z_i^{s+1}, \end{aligned} \qquad \forall i\in V, t\in[T], s\in[t-1], \quad \text{(EC.3a)}$$

$$\begin{aligned} &v_{i,t}^{s,k}\leq v_{i,t}^{s+1,k-1}+z_i^s,\\ &v_{i,t}^{s,k}\geq v_{i,t}^{s+1,k-1}-z_i^s, \end{aligned} \qquad \forall i\in V, t\in[T], s\in[t-2], k\in[t-s-1], \quad \text{(EC.3b)}$$

$$\begin{aligned} &v_{i,t}^{s,k}\leq v_{i,t}^{s+1,k}+(1-z_i^s),\\ &v_{i,t}^{s,k}\geq v_{i,t}^{s+1,k}-(1-z_i^s), \end{aligned} \qquad \forall i\in V, t\in[T], s\in[t-2], k\in[t-s-1], \quad \text{(EC.3c)}$$

$$\begin{aligned} &v_{i,t}^{s,t-s}\geq v_{i,t}^{s+1,t-s-1}-z_i^{s+1},\\ &v_{i,t}^{s,t-s}\leq v_{i,t}^{s+1,t-s-1},\\ &v_{i,t}^{s,t-s}\leq 1-z_i^{s+1}, \end{aligned} \qquad \forall i\in V, t\in[T], s\in[t-1], \quad \text{(EC.3d)}$$

$$v_{i,t}^{s,k} \geq 0, \qquad \forall i \in V, t \in [T], s \in \{0\} \cup [t], k \in \{0\} \cup [t-s]. \quad \text{(EC.3e)}$$

In this linear version of the bilinear system outlined in (EC.2), the constraint (EC.3a) corresponds to the bilinear constraint (EC.2b). Similarly, (EC.3b) and (EC.3c) are analogous to (EC.2c), and (EC.3d) aligns with (EC.2d). For brevity, we present a result from this formulation in Proposition EC.2 without proof, as it follows directly from Glover (1975).

PROPOSITION EC.2. *If $z_i^t \in \{0,1\}$ for all $i \in V$ and $t \in [T]$, then system (EC.2) is equivalent to (EC.2a) with (EC.3).*

Proposition EC.2 can be verified by imposing conditions either $z_i^{s+1} = 0$ or $z_i^{s+1} = 1$, and then comparing the respective relationship between the equations in (EC.2) and (EC.3) as pointed above.

It is useful to recall at this point the constraints of **BDM**, as they are common to all of our models in this paper:

$$x_i^{t+1} \geq \alpha_i x_i^t, \qquad \forall i \in V, t \in [T], \quad \text{(EC.4a)}$$

$$x_i^{t+1} \geq \gamma_i x_i^t + (1-\gamma_i) L_i^{\max} - (1 - \min\{\gamma_i, \alpha_i\}) L_i^{\max} z_i^t, \qquad \forall i \in V, t \in [T], \quad \text{(EC.4b)}$$

$$z_i^t = 0, \qquad \forall i \in V, t \in [t_i^{\text{start}}], \quad \text{(EC.4c)}$$

$$\sum_{s=t}^{\min\{t+t_i^{\min}, T\}} z_i^s \leq 1, \qquad \forall i \in V, \; t \in [\max\{T - t_i^{\min}, 1\}] \setminus [t_i^{\text{start}}], \quad \text{(EC.4d)}$$

$$\sum_{i \in V} c_i^t z_i^t \leq b^t, \qquad \forall t \in [T], \quad \text{(EC.4e)}$$

$$x_i^t \geq 0, \qquad \forall i \in V, t \in [T+1], \quad \text{(EC.4f)}$$

$$z_i^t \in \{0,1\}, \qquad \forall i \in V, t \in [T], \quad \text{(EC.4g)}$$

We thus arrive at the following formulation for the base deterministic model with noisy fuel dynamics ($\mathbf{x} = (x_i^t)_{i \in V, t \in [T+1]}$, $\mathbf{v} = (v_{i,t}^{s,k})_{i \in V, t \in [T], s \in [t], k \in \{0,\ldots,t-s\}}$, $\tilde{\mathbf{y}} = (\tilde{y}_i^t)_{i \in V, t \in [T+1]}$):

$$\begin{aligned} \underset{\mathbf{x},\tilde{\mathbf{y}},\mathbf{z},\mathbf{v}}{\text{minimize}} \quad & f(\mathbf{x} + \tilde{\mathbf{y}}) \\ \text{subject to} \quad & \text{(EC.4)}, \text{(Noise)}, \text{(EC.2a)}, \text{(EC.3)}. \end{aligned} \qquad \textbf{(BNM)}$$

REMARK EC.2. Note that the required number of variables v can be significantly decreased. Indeed, note that by (EC.4c), the number of treatments in a given area throughout the time horizon is at most $\lceil T/t_i^{\min} \rceil$. Thus, we have $v_{i,t}^{s,k} = 0$ for all $k < t - s - \lceil T/t_i^{\min} \rceil$, and we can drop these variables from the model. Using this remark, we can reduce the size of the formulations, by considering at most $O(T/t_i^{\min})$ for the k indices of variable $\mathbf{v}$, see Table EC.2 in Section EC.2 of this E-companion. □

EC.5 Example of (13) and the proof of Proposition 1

EXAMPLE EC.1. Let $T = 3$ and $|V| = 1$. Then, we have that the constraint (13) is constructed as follows:

$$
\begin{aligned}
&(\delta^{3,2}, \eta^{3,2}) = (\delta^{2,2}, \eta^{2,2}), \quad (\delta^{3,1}, \eta^{3,1}) = (\delta^{2,1}, \eta^{2,1}), \quad (\delta^{2,1}, \eta^{2,1}) = (\delta^{1,1}, \eta^{1,1}),\\
&\delta^{3,3} + \delta^{3,2} + \delta^{3,1} \le \Gamma^{3,\delta}(\mathbf{z}), \quad \eta^{3,3} + \eta^{3,2} + \eta^{3,1} \le \Gamma^{3,\eta}(\mathbf{z}),\\
&\delta^{2,2} + \delta^{2,1} \le \Gamma^{2,\delta}(\mathbf{z}), \quad \eta^{2,2} + \eta^{2,1} \le \Gamma^{2,\eta}(\mathbf{z}), \quad \delta^{1,1} \le \Gamma^{1,\delta}(\mathbf{z}), \quad \eta^{1,1} \le \Gamma^{1,\eta}(\mathbf{z}),\\
&0 \le \delta^{3,3}, \eta^{3,3}, \delta^{3,2}, \eta^{3,2}, \delta^{3,1}, \eta^{3,1}, \delta^{2,2}, \eta^{2,2}, \delta^{2,1}, \eta^{2,1}, \delta^{1,1}, \eta^{1,1} \le 1. \qquad \square
\end{aligned}
$$

PROPOSITION 1 *Under Assumption 1, the optimal value of **CRM** provides an upper bound for **IRM**.*

Proof. Suppose the values of $\mathbf{x}, \mathbf{z}, \mathbf{v}$ are known and fixed, and (δ^*, η^*) is optimal for the inner maximization problem of **IRM**. Since $f(\mathbf{x}+\tilde{\mathbf{y}})$ is monotone non-decreasing in $\tilde{\mathbf{y}}$, we have that any solution

$$
\begin{aligned}
\hat{y}_i^{t+1} &= \sum_{s=1}^{t} \left(((1-\alpha_i)\delta_i^{t,s} x_i^s z_i^s + (1-\gamma_i) L_i^{\max} \eta_i^{t,s} (1 - z_i^s)) \sum_{k=0}^{t-s} \gamma_i^k v_{i,t}^{s,k} \right) \\
&\ge \sum_{s=1}^{t} \left(((1-\alpha_i)\delta_i^{*s} x_i^s z_i^s + (1-\gamma_i) L_i^{\max} \eta_i^{*s} (1 - z_i^s)) \sum_{k=0}^{t-s} \gamma_i^k v_{i,t}^{s,k} \right) \\
&= \tilde{y}_i^{t+1}, \quad \forall i \in V, t \in [T],
\end{aligned}
\tag{EC.5}
$$

also satisfies $f(\mathbf{x}+\hat{\mathbf{y}}) \ge f(\mathbf{x}+\tilde{\mathbf{y}})$, see (Noise). Now, suppose that the inner maximization in **CRM** has an optimal solution $(\bar{\delta}, \bar{\eta})$ given fixed values of $\mathbf{x}, \mathbf{z}, \mathbf{v}$, which does not satisfy (EC.5). It follows that there exist $i \in V$ and $t \in [T]$ such that the left-hand side of (EC.5) is strictly smaller than the right-hand side. Now, observe that $(\delta_i^{*[t]}, \eta_i^{*[t]}) \in \Delta_i^t(\mathbf{z}_i)$, by definition. Hence, replacing the values of $\bar{\delta}_i^{t,[t]}$ and $\bar{\eta}_i^{t,[t]}$ with the values of $\delta_i^{*[t]}$ and $\eta_i^{*[t]}$, respectively, provides a feasible solution with strictly larger value of $\hat{y}_i^{t+1}$ and where every other component of $\hat{\mathbf{y}}$ is the same as before. We can repeat this reconstruction of the solution until (EC.5) is satisfied. Since $(\bar{\delta}, \bar{\eta})$ remains optimal, we have $f(\mathbf{x}+\hat{\mathbf{y}}) \ge f(\mathbf{x}+\tilde{\mathbf{y}})$, i.e., for any fixed treatment policy the inner max evaluation in **CRM** provides an upper bound of the inner max evaluation in **IRM**. ■

EC.6 Robust Mixed Integer Reformulation of Conservative Approximation

In Section 3 the full linearization of **CRM** is omitted for brevity. In this section we complete the analysis and obtain an MIP model. At the end of Section 3.2, we obtain the following reformulation of **CRM**:

$$
\underset{\mathbf{x},\mathbf{y},\mathbf{z},\mathbf{v},\omega,\sigma,\xi,\zeta}{\text{minimize}} \quad f(\mathbf{x}+\mathbf{y}) \qquad \text{(Single-level-CRM)}
$$

subject to (EC.4), (v-def),

$$\sigma_i^t + \zeta_i^{t,s} \geq (1-\gamma_i) L_i^{\max} (1 - z_i^s) \sum_{k=0}^{t-s} \gamma_i^k v_{i,t}^{s,k}, \qquad \forall i \in V,\, t \in [T],\, s \in [t], \tag{EC.6a}$$

$$\omega_i^t + \xi_i^{t,s} \geq (1-\alpha_i) x_i^s z_i^s \sum_{k=0}^{t-s} \gamma_i^k v_{i,t}^{s,k}, \qquad \forall i \in V,\, t \in [T],\, s \in [t], \tag{EC.6b}$$

$$\omega_i^t, \sigma_i^t, \xi_i^{t,s}, \zeta_i^{t,s} \geq 0, \qquad \forall i \in V,\, t \in [T], s \in [t], \tag{EC.6c}$$

$$y_i^{t+1} = \Gamma_i^{t,\delta}(\mathbf{z}_i)\omega_i^t + \Gamma_i^{t,\eta}(\mathbf{z}_i)\sigma_i^t + \sum_{s=1}^{t} (\xi_i^{t,s} + \zeta_i^{t,s}), \qquad \forall i \in V,\, t \in [T]. \tag{EC.6d}$$

Observe that Single-level-**CRM** is non-linear. In particular, constraints (EC.6a) and (EC.6b), include the terms $v_{i,t}^{s,k} z_i^s$ and $v_{i,t}^{s,k} z_i^s x_i^t$, respectively. Since $\Gamma_i^{t,\delta}(\mathbf{z}_i) = \Gamma_i^{t-1,\delta}(\mathbf{z}_i) + \beta_i^{t,\delta}(1 - z_i^t)$ and $\Gamma_i^{t,\eta}(\mathbf{z}_i) = \Gamma_i^{t-1,\eta}(\mathbf{z}_i) + \beta_i^{t,\eta}(1 - z_i^t)$, we have that (EC.6d) is equivalent to

$$\begin{aligned} y_i^{t+1} &= \left(\sum_{s=1}^{t} (\beta_{i,\delta}^s (1 - z_i^s)) + \Gamma_{i,\delta}^0 \right) \omega_i^t + \left(\sum_{s=1}^{t} (\beta_{i,\eta}^s (1 - z_i^s)) + \Gamma_{i,\eta}^0 \right) \sigma_i^t + \sum_{s=1}^{t} (\xi_i^{t,s} + \zeta_i^{t,s}) \\ &= \sum_{s=1}^{t} ((\beta_{i,\delta}^s \omega_i^t + \beta_{i,\eta}^s \sigma_i^t)(1 - z_i^s)) + \Gamma_{i,\delta}^0 \omega_i^t + \Gamma_{i,\eta}^0 \sigma_i^t + \sum_{s=1}^{t} (\xi_i^{t,s} + \zeta_i^{t,s}), \quad \forall i \in V,\, t \in [T]. \end{aligned} \tag{EC.7}$$

Hence, we also need to linearize the products $(1 - z_i^s)\omega_i^t$ for $s \in [t]$ in (EC.7). Our derivations allow us to obtain a compact MIP formulation for **CRM**. This implies that our reformulation keeps the tractability of the deterministic model presented in Section 2.2. Thus, we reformulate these products by introducing new variables and employing a standard approach to obtain a linear model; see Glover (1975), McCormick (1976). Specifically, we define

$$\pi_{i,t}^{s,k} = v_{i,t}^{s,k}(1 - z_i^s), \tag{EC.8a}$$

$$u_i^t = z_i^t x_i^t, \tag{EC.8b}$$

$$\chi_{i,t}^{s,k} = v_{i,t}^{s,k} u_i^t, \tag{EC.8c}$$

$$\lambda_i^{t,s} = (\beta_{i,\delta}^s \omega_i^t + \beta_{i,\eta}^s \sigma_i^t)(1 - z_i^s). \tag{EC.8d}$$

Observe that each equation in (EC.8) is a product of a binary variable with a non-negative bounded variable. This ensures that the reformulation we obtain is exact.

Finally, using the reformulation obtained in Section EC.4, we know that (v-def) can be modeled using (EC.2a), (EC.3). Hence, our robust MIP reformulation for **CRM** is:

$$\underset{\substack{\mathbf{x},\mathbf{y},\mathbf{z},\mathbf{v},\mathbf{u},\\ \lambda,\chi,\pi,\omega,\sigma,\xi,\zeta}}{\text{minimize}} \quad f(\mathbf{x}+\mathbf{y}) \tag{**RMIP**}$$

subject to (EC.4), (EC.6c), (EC.2a), (EC.3),

$$\sigma_i^t + \zeta_i^{t,s} \geq (1-\gamma_i) L_i^{\max} \sum_{k=0}^{t} \gamma_i^k \pi_{i,t}^{s,k}, \qquad \forall i \in V,\, t \in [T],\, s \in [t], \tag{EC.9a}$$

$$\begin{aligned} v_{i,t}^{s,k} - z_i^s \le \pi_{i,t}^{s,k} \le v_{i,t}^{s,k}, \\ \pi_{i,t}^{s,k} \le 1 - z_i^s, \end{aligned} \qquad \begin{aligned} &\forall i \in V, t \in [T], s \in [t], \\ &k \in \{0, \dots, t-s\}, \end{aligned} \tag{EC.9b}$$

$$\omega_i^t + \xi_i^{t,s} \ge (1-\alpha_i) \sum_{k=0}^{t-s} \gamma_i^k \chi_{i,t}^{s,k}, \qquad \forall i \in V,\ t \in [T],\ s \in [t], \tag{EC.9c}$$

$$\begin{aligned} 0 \le u_i^t \le L_i^{\max} z_i^t, \\ x_i^t - L_i^{\max}(1 - z_i^t) \le u_i^t \le x_i^t, \end{aligned} \qquad \forall i \in V, t \in [T], \tag{EC.9d}$$

$$\begin{aligned} 0 \le \chi_{i,t}^{s,k} \le L_i^{\max} v_{i,t}^{s,k}, \\ u_i^s - L_i^{\max}(1 - v_{i,t}^{s,k}) \le \chi_{i,t}^{s,k} \le u_i^s, \end{aligned} \qquad \begin{aligned} &\forall i \in V, t \in [T], s \in [t], \\ &k \in \{0, \dots, t-s\}, \end{aligned} \tag{EC.9e}$$

$$y_i^{t+1} = \sum_{s=1}^{t} (\lambda_i^{t,s} + \xi_i^{t,s} + \zeta_i^{t,s}) + \Gamma_i^{0,\delta} \omega_i^t + \Gamma_i^{0,\eta} \sigma_i^t, \qquad \forall i \in V,\ t \in [T], \tag{EC.9f}$$

$$\begin{aligned} 0 \le \lambda_i^{t,s} \le (\beta_{i,\delta}^s + \beta_{i,\eta}^s) L_i^{\max}(1 - z_i^s), \\ (\beta_{i,\delta}^s \omega_i^t + \beta_{i,\eta}^s \sigma_i^t) - (\beta_{i,\delta}^s + \beta_{i,\eta}^s) L_i^{\max} z_i^s \le \lambda_i^{t,s}, \\ \lambda_i^{t,s} \le (\beta_{i,\delta}^s \omega_i^t + \beta_{i,\eta}^s \sigma_i^t), \end{aligned} \qquad \forall i \in V,\ t \in [T], s \in [t]. \tag{EC.9g}$$

In this reformulation, constraints (EC.9a) and (EC.9b) linearize the bilinear terms $v_{i,t}^{s,k} z_i^s$ in (EC.6a). Note that (EC.9b) corresponds to (EC.8a). Similarly, (EC.9c), (EC.9d) and (EC.9e) linearize terms $v_{i,t}^{s,k} z_i^s x_i^t$ in (EC.6b). Here (EC.9d) and (EC.9e) correspond to (EC.8b) and (EC.8c), respectively. In addition, constraint (EC.9f) corresponds to (EC.6d). Finally, (EC.9g) enforces the definition introduced in (EC.8d).

EC.7 Reformulation ideal robust model total fuel load minimization

For the fuel load minimization, i.e., minimizing $f(\mathbf{x}, \mathbf{z}, \mathbf{v})$ in (18), as mentioned previously in Section 4.2, **IRM** can be optimized directly without the need to approximate the lower level problem. The resulting formulation is very similar to **RMIP** since the linearization approach is the same. Below we present the resulting linear MIP formulation:

$$\begin{aligned} \underset{\substack{\mathbf{x},\mathbf{z},\mathbf{v},\mathbf{u},\\ \lambda,\chi,\pi,\omega,\sigma,\xi,\zeta}}{\text{minimize}} \quad & \sum_{i \in V, t \in [T+1]} \left(x_i^t + \sum_{s=1}^{t} (\lambda_i^{t,s} + \tilde{\xi}_i^s + \tilde{\zeta}_i^s) + \Gamma_i^{0,\delta} \omega_i^t + \Gamma_i^{0,\eta} \sigma_i^t \right) \\ \text{subject to} \quad & (\text{EC.4}), (\text{EC.2a}), (\text{EC.3}), \\ & (\text{EC.9b}), (\text{EC.9d}), (\text{EC.9e}), (\text{EC.9g}), \end{aligned}$$

$$\sum_{t=s}^{T} \sigma_i^t + \tilde{\zeta}_i^s \ge (1 - \gamma_i) L_i^{\max} \sum_{k=0}^{t} \gamma_i^k \pi_{i,t}^{s,k}, \qquad \forall i \in V,\ s \in [T], \tag{EC.10a}$$

$$\sum_{t=s}^{T} \omega_i^t + \tilde{\xi}_i^s \ge (1 - \alpha_i) \sum_{k=0}^{t-s} \gamma_i^k \chi_{i,t}^{s,k}, \qquad \forall i \in V,\ s \in [T], \tag{EC.10b}$$

$$\omega_i^s, \sigma_i^t, \tilde{\xi}_i^s, \tilde{\zeta}_i^s \ge 0 \qquad \forall i \in V,\ s \in [T]. \tag{EC.10c}$$

The expression for the objective function of (EC.10) is the same as in (18) after linearization, whereas all the constraints, except for (EC.10a)-(EC.10c), which is a linearized expression of (Ideal-dual), are the same as in the system to formulate **RMIP**.

node id (i)	t_i^{init}	x_i^1	node id (i)	t_i^{init}	x_i^1	node id (i)	t_i^{init}	x_i^1	node id (i)	t_i^{init}	x_i^1
1	28	16.28	10	33	16.35	19	24	16.17	28	30	16.32
2	31	16.33	11	9	13.40	20	16	15.49	29	30	16.32
3	8	12.85	12	26	16.23	21	9	13.40	30	17	15.63
4	17	15.63	13	17	15.63	22	14	15.12	31	14	15.12
5	17	15.63	14	34	16.36	23	14	15.12	32	14	15.12
6	33	16.35	15	24	16.17	24	24	16.17	33	16	15.49
7	17	15.63	16	8	12.85	25	14	15.12	34	2	6.55
8	8	12.85	17	42	16.39	26	18	15.75			
9	33	16.35	18	24	16.17	27	30	16.32			

Table EC.3 Initial maturities t_i^{init} and initial fuel loads (x_i^1) of the locations considered in Example 2 and Section 5. The calculation of initial fuel loads is given by $x_i^1 = L^{\max}(1-\exp(-\kappa(t_i^{\text{init}}+1)))$.

EC.8 Initial maturities

For completeness and reproducibility, we provide in Table EC.3 the initial maturities and fuel loads used in the case study, described in Example 2 and Section 5. These values were also used in Matsypura et al. (2018). To compute the initial fuel loads from these values, we assume an initial post fire state $L^{\text{init}} = 0$ and calculate the resulting load using (2) after $t_i^{\text{init}}+1$ years of uninterrupted fuel growth.

EC.9 Additional computational results

In this section, we present the remaining results for combinations of $\hat{\beta}^\delta, \hat{\beta}^\eta \in \{0, 0.01, 0.02, 0.05\}$ and the scalability results not included in Section 5. Our scalability study uses both the real instance described in Section 5.1 with a time horizon of $T = 14$ as well as randomly generated synthetic instances, described later. Each instance was run with a time limit of two hours.

EC.9.1 Additional robust policies and optimization results in Hawkesbury

We first discuss results of the real instance. Table EC.4 presents our results for different values of $\hat{\beta}^\delta, \hat{\beta}^\eta$. We ran the model of Matsypura et al. (2018) only with $\hat{\beta}^\delta = \hat{\beta}^\eta = 0$ (the deterministic setting) since no robust version of this model exists. Table EC.4 reports solution times in seconds for instances that reached the default Gurobi optimality tolerance (0.01%), and also the reported optimality gap as a percentage for instances that hit the time limit. These results show the clear superiority of our model with respect to the previous one for our case study in the Hawkesbury region.

Figures EC.1 and EC.2 present the complete mismatch–loss results for all the objectives considered. These results support our conclusions from Section 5. For the fuel-load objective, overspecifying uncertainty raises loss but it collapses once treatment-effect uncertainty is reduced to moderate levels; when fuel-growth noise is near zero, increasing uncertainty of treatment effect incurs in high mismatch losses. For the active-edges objective, penalties decline only when both uncertainty sources are small, after which robust plans behave comparably to deterministic ones.

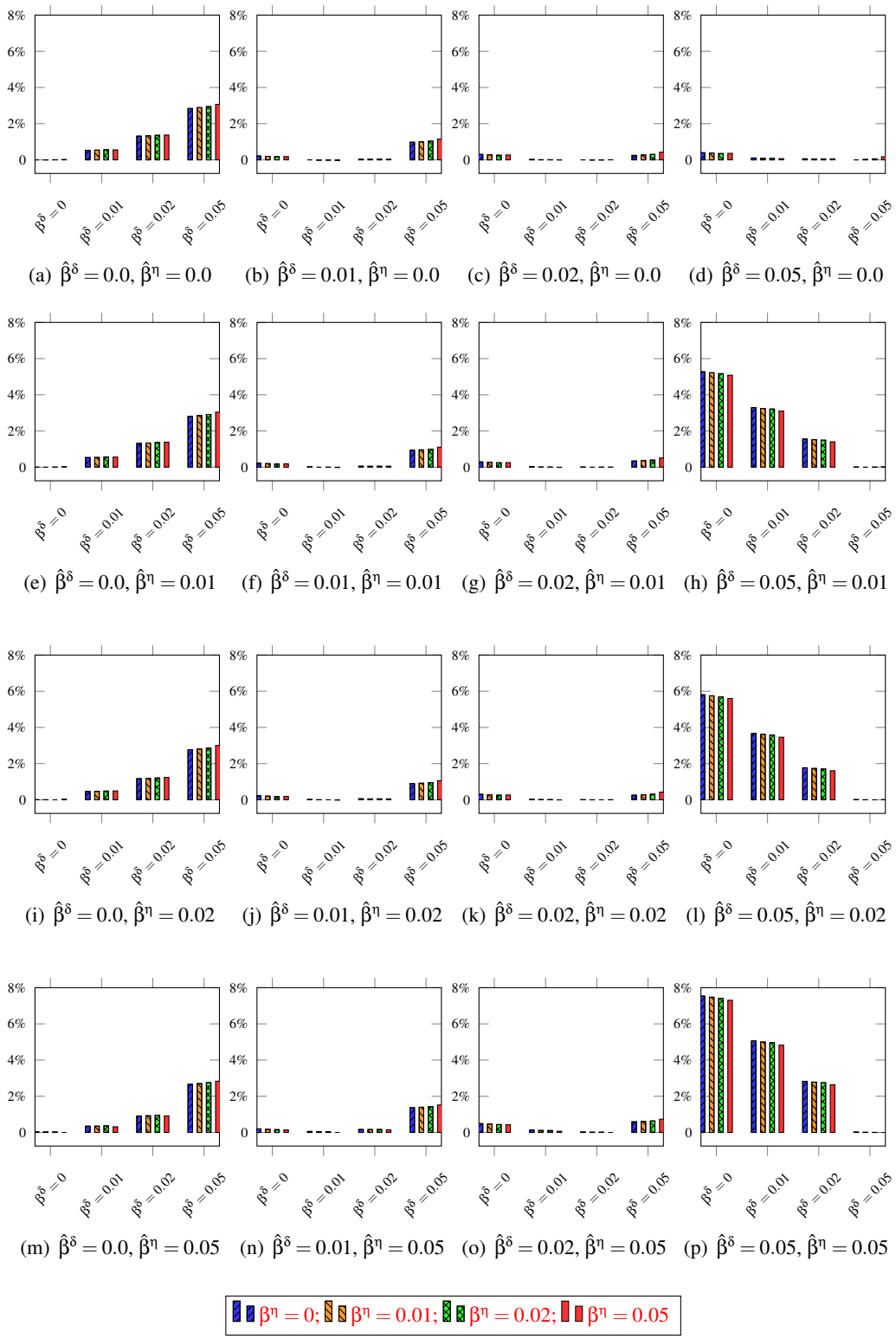

Figure EC.1 MML (mismatch loss) values for the total fuel load objective, averaged over different budgets $b_t = 1, 3, 5$.

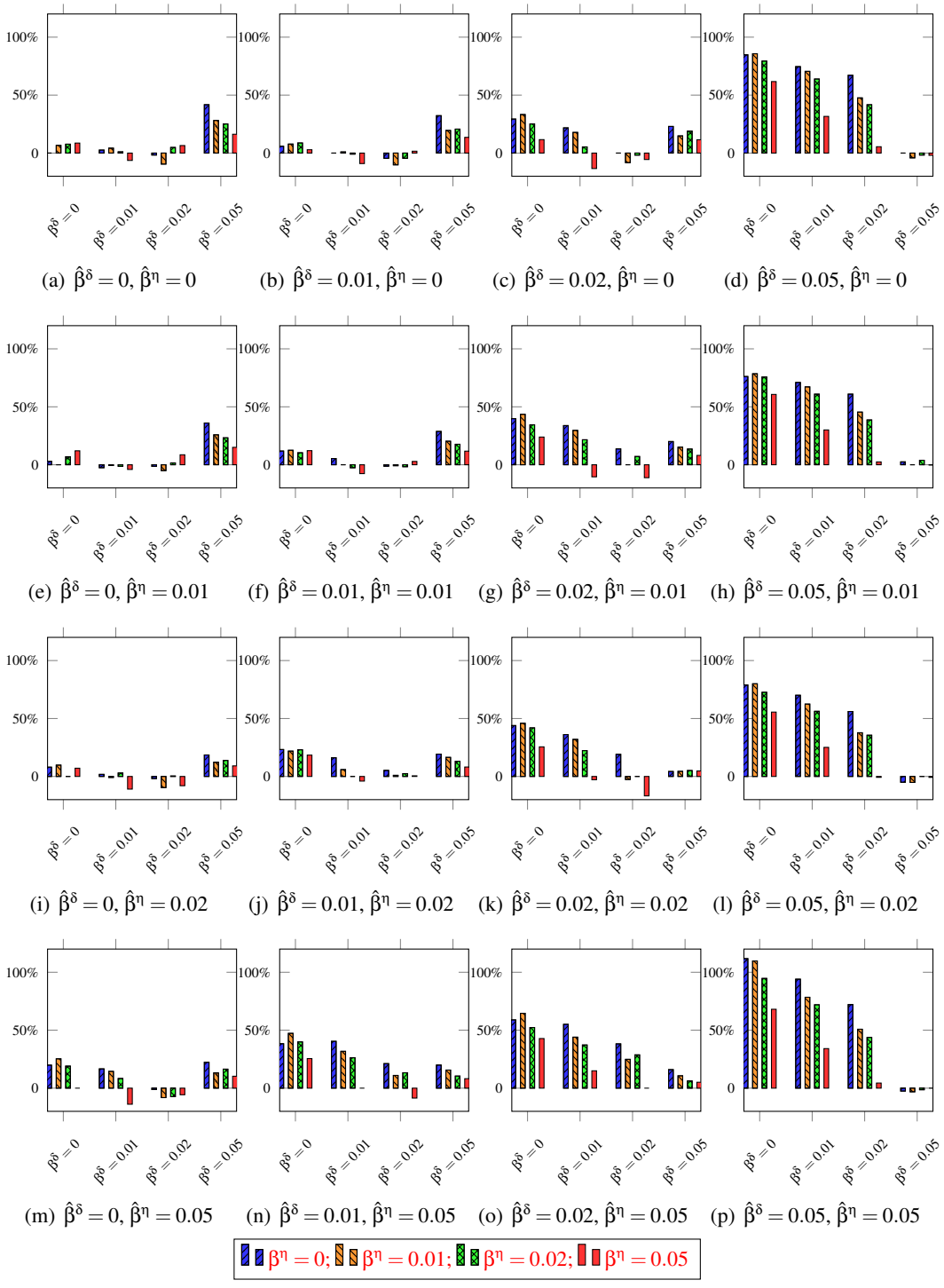

Figure EC.2 MML (mismatch loss) values for the number of active edges objective, averaged over different budgets $b_t = 1, 3, 5$.

Objective	b_t	Matsypura et al. (2018)	$\hat{\beta}^\delta = 0, \hat{\beta}^\eta = 0$	$\hat{\beta}^\delta = 0.02, \hat{\beta}^\eta = 0$	$\hat{\beta}^\delta = 0, \hat{\beta}^\eta = 0.02$	$\hat{\beta}^\delta = 0.02, \hat{\beta}^\eta = 0.02$
Total fuel load	1	3.55%	<1	1.30%	22	1.56%
	3	10.24%	<1	6.14%	0.07%	6.61%
	5	12.99%	<1	4.22%	17	5.69%
Number of active edges	1	29.31%	14	9.67%	74	15.30%
	3	47.90%	10	51.37%	11.84%	47.12%
	5	46.95%	<1	49.86%	6.60%	43.99%

Table EC.4 Solution time (in seconds) and optimality gap (in % at the two-hour limit) on the real instance with $T = 14$ and $b_t \in \{1, 3, 5\}$. The column labeled Matsypura et al. (2018) reports results on the previous equivalent formulation when $(\hat{\beta}^\delta, \hat{\beta}^\eta) = (0, 0)$ in the deterministic case.

EC.9.2 Random instances generation

To generate a random instance, we first generate a random planar graphs as follows. We sample a number of points from the unit square, and construct a Voronoi diagram, which partitions the unit square. Vertices of the Voronoi diagram (points in the square that are equidistant to three or more sampled points) become graph vertices. Edges of the diagram become edges of the graph as well; only edges with both endpoints in the unit square are used. This procedure is used to generate three different network topologies with $(|V|, |E|) \in \{(20, 26), (51, 68), (101, 138)\}$. Once the planar graph is generated, we generate instances by assigning different initial maturities to each vertex, generated as a random integer between 1 and 40. For each graph, 10 sets of initial maturities were generated, thus giving us 30 instances overall. For each random instance, we solve our model with time horizons $T \in \{14, 19\}$, budgets $b_t \in \{\lfloor 0.05|V| \rfloor, \lfloor 0.1|V| \rfloor, \lfloor 0.15|V| \rfloor\}$, and uncertainty budgets $(\hat{\beta}^\delta, \hat{\beta}^\eta) \in \{(0, 0), (0.05, 0), (0, 0.05), (0.05, 0.05)\}$. Therefore, for each instance we solve 24 different models.

EC.9.3 Scalability study random instances

In this section, we test the scalability of our models for the random instances generated using the methodology described in Section EC.9.2. In the deterministic setting (without robustness) our models are equivalent to that of Matsypura et al. (2018), though with much fewer variables and constraints. To enable comparison of the benefit of our new model, we test the old model of Matsypura et al. (2018) on deterministic instances. It is known that adding robustness makes models more complex as compared to their deterministic counterparts, therefore we test to what extent we can reasonably solve our robust formulations.

Table EC.5 reports the results for the total fuel load objective. For each graph and parameter combination $(T, b_t, \hat{\beta}^\delta, \hat{\beta}^\eta)$, the average solution time is reported when all 10 instances of initial maturities solved to optimality within the two-hour limit; otherwise, the average optimality gap is reported. (It turned out that on all combinations, either all instances solved, or all instances did not solve.) For the deterministic case $(\hat{\beta}^\delta, \hat{\beta}^\eta) = (0, 0)$ we see from Table EC.5 that our model is able to

			Objective: total fuel load				
$\|V\|$	T	b_t	Matsypura et al. (2018)	$\hat{\beta}^{\delta}=0, \hat{\beta}^{\eta}=0$	$\hat{\beta}^{\delta}=0.05, \hat{\beta}^{\eta}=0$	$\hat{\beta}^{\delta}=0, \hat{\beta}^{\eta}=0.05$	$\hat{\beta}^{\delta}=0.05, \hat{\beta}^{\eta}=0.05$
20	14	1	4.90%	<1	2.98%	522	4.15%
		2	9.59%	2	4.90%	1075	5.12%
		3	13.12%	<1	4.79%	533	5.24%
	19	1	14.48%	31	5.83%	0.20%	7.62%
		2	19.66%	6	11.18%	0.24%	12.51%
		3	20.36%	2	9.50%	0.19%	10.45%
51	14	2	5.69%	2	3.08%	0.14%	3.79%
		5	12.30%	4	7.30%	0.09%	8.23%
		7	13.35%	2	6.04%	0.07%	7.11%
	19	2	12.35%	25	5.90%	0.48%	7.28%
		5	21.66%	23	12.04%	0.45%	14.52%
		7	21.93%	16	11.61%	0.36%	13.70%
101	14	5	8.25%	7	5.51%	0.28%	6.57%
		10	14.07%	13	8.82%	0.13%	10.23%
		15	15.96%	10	7.75%	0.09%	9.35%
	19	5	17.43%	455	8.16%	0.81%	10.04%
		10	26.37%	52	14.15%	0.86%	15.92%
		15	25.38%	23	12.84%	0.70%	14.33%

Table EC.5 Average solution time (in seconds) and average optimality gap (in % at the two-hour limit) on synthetic instances. The column labeled Matsypura et al. (2018) reports results on the previous equivalent formulation when $(\hat{\beta}^{\delta}, \hat{\beta}^{\eta}) = (0,0)$ in the deterministic case.

solve all instances to optimality within five minutes on average, many of which solve within seconds. In contrast, the previous model was not able to solve any to optimality. When robustness is added, the computation becomes more challenging, and for the majority of parameter combinations our model does not solve to optimality. However, the optimality gaps are reasonable, no more than 16%, and often less than 10%. In particular, the optimality gaps for the robust settings are lower than the model of Matsypura et al. (2018) for the deterministic setting. These results further demonstrate the superior scalability of our new formulation, as well as the tractability of the new robust framework.

Table EC.6 is analogous to Table EC.5 except it is for the number of active edges. The results in Table EC.6 indicate that increasing uncertainty in the fuel load ($\hat{\beta}^{\eta}$) makes it harder to find feasible solutions within the two hour limit than increasing uncertainty in treatment effect ($\hat{\beta}^{\delta}$). That said, when feasible solutions are found, lower optimality gaps are reported for uncertainty in fuel growth. In summary, the scalability results suggest that our robust optimization framework can be used for the fuel load and active edge objectives.

			Objective: number of active edges			
$\|V\|$	T	b_t	$\hat{\beta}^{\delta}=0, \hat{\beta}^{\eta}=0$	$\hat{\beta}^{\delta}=0.05, \hat{\beta}^{\eta}=0$	$\hat{\beta}^{\delta}=0, \hat{\beta}^{\eta}=0.05$	$\hat{\beta}^{\delta}=0.05, \hat{\beta}^{\eta}=0.05$
20	14	1	419s (10) –	5000s (3) 11.68% (7)	2670s (10) –	3958s (10) –
		2	14s (10) –	3123s (10) –	4462s (4) 5.41%(6)	2464s (10) –
		3	4s (10) –	2185s (10) –	4331s (10) –	1500s (10) –
	19	1	2990s (4) 2.85% (6)	– 45.85% (10)	– 10.72% (10)	– 21.16% (10)
		2	50s (10) –	– 59.56% (10)	– 22.86% (10)	– 33.95% (10)
		3	12s (10) –	– 53.99% (10)	– 21.35% (10)	6410s (1) 28.22% (9)
51	14	2	1795s (10) –	– 20.52% (10)	– 1.26% (10)	6331s (2) 9.67% (8)
		5	160s (10) –	– 44.69% (10)	– 10.12% (10)	5895s (2) 8.46% (8)
		7	25s (10) –	– 33.85% (10)	– 8.88% (10)	4510s (3) 2.19% (7)
	19	2	– 10.42% (10)	– 42.12% (10)	– 14.4% (10)	– 30.19% (10)
		5	654s (10) –	– 81.23% (10)	– 55.39% (10)	– 80.96% (10)
		7	111s (10) –	– 80.34% (10)	– 48.45% (10)	– 70.48% (10)
101	14	5	– 6.2% (10)	– 37.72% (10)	– 11.33% (10)	– 19.66% (10)
		10	2374s (9) 1.07%(9)	– 68.0% (10)	– 25.9% (10)	– 57.51% (10)
		15	375s (10) –	– 61.5% (10)	– 24.65% (10)	– 30.14% (10)
	19	5	– 18.7% (10)	– 59.36% (10)	– –	– 58.55% (10)
		10	5098s (1) –	– 86.35% (10)	– –	– –
		15	709s (10) –	– 86.12% (10)	– –	– 84.23% (6)

Table EC.6 Average solution times and optimality gaps for computing policies under varying levels of uncertainty for the active edges objective ($\|\varepsilon\|_1$), using synthetic instances. Each cell reports the following in a two-line format: the average time in seconds and the number of instances solved to optimality within the two-hour time limit (first line); and the average optimality gap (in %) and the number of instances for which a feasible solution was found within the time limit (second line). A "–" indicates that the corresponding value is not applicable (i.e., all instances solved to optimality, no instance solved to optimality or no feasible solutions found). Each entry is based on 10 instances. The four columns for each objective correspond to different values of $\hat{\beta}^{\delta}$ and $\hat{\beta}^{\eta}$, i.e., to get the first column we solve **BDM**, while for the others we solve the linearization of **CRM** given by **RMIP**.